Cell type specific analysis of ALS-associated proteins reveals immune-regulated targets

Riham Ayoubi[1,2], Emma J. MacDougall[1,2], Ian McDowell[1,2], Marie-France Dorion[3], Jay P. Ross[4], Sara González Bolívar[1,2], Vera Ruiz Moleón[1,2], Charles Alende[1,2], Maryam Fotouhi[1,2], Mathilde Chaineau[1,3], Carol X.-Q. Chen[1,3], Valerio E.C. Piscopo[1,3], Vincent Soubannier[1,3], Gilles Maussion[1,3], Cecilia Rocha[1,3], Tracy Keates[5], Wen Hwa Lee[5], Brian D. Marsden[6], Leonidas Koukouflis[6], Edvard Wigren[7], Carolyn A. Marks[7], Luke M. Healy[8], Patrick A. Dion[2], Guy A. Rouleau[1,2], Edward A. Fon[1,2], Susanne Gräslund[7], Opher Gileadi[5,7], Aled M. Edwards[1], Thomas M. Durcan[1,3], Peter S. McPherson[1,2], Carl Laflamme[1,2]

Author affiliations:

[1]Structural Genomics Consortium, Montreal Neurological Institute-Hospital (The Neuro), McGill University, Montreal, H3A 2B4, Canada.

[2]Neurodegenenerative Diseases Research Group, Department of Neurology and Neurosurgery, Montreal Neurological Institute-Hospital (The Neuro), McGill University, Montreal, H3A 2B4, Canada.

[3]Early Drug Discovery Unit (EDDU), Department of Neurology and Neurosurgery, Montreal Neurological Institute-Hospital (The Neuro), McGill University, Montreal, H3A 2B4, Canada.

[4]Department of Genetics, Stanford University School of Medicine, Stanford, CA, 94305, USA

[5]Structural Genomics Consortium, Nuffield Department of Medicine, University of Oxford, Oxford, OX3 7FZ, UK

[6]Nuffield Department of Medicine, University of Oxford, Oxford, OX3 7FZ, UK.

[7]Structural Genomics Consortium, Department of Medicine, Karolinska Institute, Solna, 171 76, Sweden

[8]Neuroimmunology Unit, Department of Neurology and Neurosurgery, Montreal Neurological Institute-Hospital (The Neuro), McGill University, Montreal, H3A 2B4, Canada.

Correspondence to: Carl Laflamme

Full address: McGill University, Montreal Neurological Institute, Room BT-205, 3801 University St.,

Montreal, QC, H3A 2B4, CANADA

E-mail: carl.laflamme@mcgill.ca

Running title: Immune-Regulated ALS Protein Targets

Keywords: oligodendrocyte; macrophage; astrocytes; interferon-gamma; lipopolysaccharide; RNA sequencing

Abstract

Genetic studies are revolutionizing our understanding of neurodegenerative diseases by identifying hundreds of new genetic risk factors, yet the ability to link these variants to phenotype is constrained by the lack of knowledge on the encoded proteins. Moreover, for any given disease, elucidating the functional connections among the genetic risk factors has been challenging. Using 33 risk genes for amyotrophic lateral sclerosis (ALS) as a model, we set out to explore connections among the encoded proteins using antibodies identified within a systematic framework exploiting knockout-based antibody characterization. We characterized 296 antibodies against 33 genetically linked to ALS—ACSL5, ALS2, ANG, ANXA11, ATXN2, C9orf72, CAV1, CCNF, CHCHD10, CHMP2B, FIG4, FUS, HNRNPA1, HNRNPA2B1, KIF5A, LGALS1, MATR3, NEK1, OPTN, PFN1, SETX, SIGMAR1, SOD1, SPG11, SQSTM1, TAF15, TARDBP, TBK1, TIA1, TUBA4A, UBQLN2, VAPB, and VCP—and identified high-quality reagents for most proteins. Using these reagents, as the first step in characterizing the ALS genetic risk proteome, we profiled protein expression across human induced pluripotent stem cell–derived and primary neurological cells. Protein-level analyses uncovered diverse and unexpected expression signatures, discordant with RNA datasets. Notably, 22 proteins were enriched in glial populations, with ten dynamically regulated by inflammatory cues in microglia, underscoring immune-responsive pathways as key contributors to ALS pathogenesis. This work provides both a reference resource for ALS biology and a generalizable framework for translating genetic discoveries into mechanistic protein insights in neurodegeneration.

Introduction

Large-scale genome-wide association and sequencing studies have identified numerous risk loci across multiple neurodegenerative diseases. Recent genome-wide association studies (GWAS) identified 134 risk loci for Parkinson's disease,[1,2] and Alzheimer's disease studies have reported 75 loci.[3,4] At least 33 genes have been linked to familial and sporadic forms of amyotrophic lateral sclerosis (ALS),[5,6] a rare but devastating motor neuron disorder with extremely poor prognosis. Yet functional follow-up remains scarce: most risk genes lack validated protein tools, hindering hypothesis generation, mechanistic validation, and translation of genetic discoveries into disease biology.

ALS illustrates this gap clearly. While four ALS-linked genes—*SOD1*, *C9orf72*, *FUS*, and *TARDBP*—have been studied intensively (accounting for 80% of total PubMed entries), the remaining 29 ALS-associated proteins remain unexplored in the context of the disease. Multiple cellular pathways have been implicated in ALS pathogenesis, including RNA metabolism, autophagy, and lysosomal function, but the contributions of ALS-linked proteins to these processes remain poorly defined. RNA-based analyses suggest glial enrichment of some ALS genes,[7] but RNA abundance is an unreliable proxy for protein expression due to post-transcriptional and translational regulation.[8-10] Validated protein recognition tools (e.g. antibodies) are therefore required to directly define where ALS proteins are expressed and how they are regulated.

To address this challenge, we established the ALS Reproducible Antibody Platform (ALS-RAP), a framework combining knockout (KO)-based antibody validation, standardized workflows, and open-science dissemination. We characterized 296 antibodies using KO cancer cell lines against 33 ALS-associated proteins and identified high-quality reagents for most targets. We then profiled protein expression across human induced pluripotent stem cell (iPSC)-derived and primary neurons, astrocytes, oligodendrocytes, microglia, and macrophages, and revealed diverse and often unexpected expression signatures, including enrichment of 22 proteins in glial populations and dynamic regulation of ten proteins by inflammatory cues in microglia. These findings highlight immune-responsive pathways as important contributors to ALS pathogenesis.

Materials and methods

Analysis of PubMed entries for each ALS-associated gene

Throughout the manuscript, we reference ALS-RAP targets using their official gene names as listed in UniProt, written in italics (e.g., *SOD1*). To refer to the corresponding proteins, we use the same gene names in regular font, as the official protein names are often too long or ambiguous for practical use.

Each target gene was queried in PubMed using two search strategies: (1) GENE_NAME[Title/Abstract] to retrieve the total number of publications associated with the gene, and (2) (GENE_NAME[Title/Abstract]) AND ("amyotrophic lateral sclerosis" [Title/Abstract]) to identify publications specifically linking the gene to ALS. Searches were performed on August 27, 2025.

Evaluation of significance of ALS-associated genes

Each candidate gene was assessed for its potential association with ALS using the evidence published at the time of this manuscript. Using the recent review of Nijs & van Damme as a model,[6] we used currently available evidence to prioritize genes for potential association with ALS in a similar manner. First, genes were qualitatively assessed for rarity of genetic variants in the general population and among individuals with ALS. Next, any reported odds ratios (OR) for risk of ALS in variant carriers were used to approximate whether genes could be considered as having "small" (OR < 1.2), "intermediate" (1.2 < OR < 10), or "high" (OR > 10) effect sizes. Genes were assigned an "uncertain" OR estimate if no OR had been published at the time of analysis. Variant frequency was assessed considering the type(s) of inheritance previously described; variants reported through GWAS or genotyping studies were designated as "common" whereas variants reported in autosomal family/pedigree-based studies were designated as "rare". If the method of discovery was poorly described or through non-genetic analyses (e.g. transcriptomic or proteomic), genes were described as having "uncertain" frequency.

RNA expression analysis

We accessed the single-cell transcriptomics resource of the Human Protein Atlas (HPA), specifically the single-nuclei brain dataset which includes single-cell RNA sequencing data generated from 2.5 million cells and mapped to 34 supercluster cell types. Data were generated from post-mortem human brain samples digested to a single cell suspension, and cell types were clustered into transcriptomic cell types.[11] Raw sequencing data was normalized using Trimmed mean of M values and expression values were presented as normalized transcripts per million (nTPM). RNA expression data for all 33 ALS genes were downloaded online from the HPA. Data were grouped together based on overall cell type (neuron, oligodendrocyte, astrocyte, microglia, etc.) and the average expression in each cell type was determined

for each gene. The average neuron, oligodendrocyte, astrocyte, and microglia expression data were extracted from the overall dataset and used in downstream analyses.

In our analyses, genes were considered “expressed” if their expression values in at least three cell types were greater than the median expression value of the entire HPA dataset (9.2 nTPM). Genes were considered “barely detectable” if expression was less than the median value in at least two cell types. For a small subset of “barely detectable” genes, expression in one cell type was greater than the median value and substantially “enriched” in that cell type. We included these in the category of “expressed” genes despite the low expression in most cell types.

To describe the cell type expression patterns for each gene, we established criteria determining if mRNA expression levels for a gene is “enriched” or not in a given cell type. Cell types in which mRNA expression for a gene is “enriched” were defined as when the ratio of the expression value in that cell type to the average expression value across all cell types was greater than or equal to 1.5*. Each gene was categorized based on the “enriched” cell types. If either more than one cell type was “enriched” or no cell types were, the gene was categorized as having “low cell-type specificity”.

$$*\frac{Expression\ value\ in\ given\ cell\ type}{Average\ across\ all\ cell\ types} \geq 1.5$$

String analysis

STRING analysis was performed by entering the UniProt IDs of the 33 ALS-RAP proteins into the “multiple proteins” search at string-db.org. The analysis was restricted to the “physical subnetwork”, with the minimum required interaction score set to “high confidence”.

Western blot

Cultured cells were collected in RIPA buffer (25mM Tris-HCl pH 7.6, 150mM NaCl, 1 % NP-40, 1% sodium deoxycholate, 0.1% SDS) supplemented with protease inhibitors. Lysates were sonicated briefly for 5-10 secs depending on the volume. Following 30 min on ice, lysates were spun at ~110,000 x *g* for 15 min at 4°C and equal protein aliquots of the supernatants were analyzed by SDS-PAGE and immunoblot. Microglia differentiated for the IFNγ and LPS or IL-4 treatments were collected in RIPA buffer supplemented with both protease and phosphatase inhibitors.

Chemiluminescent western blotting

Immunoblots were performed with precast 10% Bis-Tris polyacrylamide gels and nitrocellulose membranes. Total proteins were visualized with a Ponceau staining. Blots were blocked with 5% milk in TBS with 0.1% Tween 20 (TBST), and antibodies were diluted in the same buffer and incubated O/N at 4°C followed by three washes. The peroxidase conjugated secondary antibody was diluted in 5% milk in TBST at 0.5-1 µg/mL and incubated with the membranes for 1 hr at room temperature followed by three

washes. Membranes were incubated with ECL for 1 min prior to detection with the iBright CL1500 Imaging System (Thermo Fisher Scientific).

Fluorescent western blotting

Immunoblots were performed with large 5–16% gradient Tris-based polyacrylamide gels and nitrocellulose membranes. Total proteins were visualized with the REVERT total protein stain (LI-COR Biosciences). Blots were blocked with 5% milk in TBST, and antibodies were diluted in the same buffer and incubated O/N at 4°C followed by three washes. The secondary antibody (Odyssey IRDye 800CW or IRDye 680RD) was diluted in 5% milk in TBST at 1:10,000-1:20,000 (0.05-0.1 µg/mL) and incubated with the membranes for 1 hr at room temperature followed by three washes. Immuno-reactive bands were detected using the LI-COR Odyssey Imaging System (LI-COR Biosciences), and data analysis was done using LI-COR Image Studio Lite Version 5.2.

iPSC differentiation protocols

Healthy control iPSCs from the AIW002-02 & QPN929 backgrounds (Early Drug Discovery Unit-EDDU, McGill University) were selected for differentiation into the indicated neurological cell types. In all cases, iPSCs were cultured in mTeSR1 for 5-7 days prior to differentiation. Two batches (named A & B) of neurological cells were generated from the AIW002-02 background using identical protocols, with the exception that the QPN929 iPSC line was used for microglia differentiation in batch B. Batch C corresponds to an independent lot of microglia differentiated specifically for stimulation experiments. All cell types and their corresponding batches are listed in the table of lysates.

Motor neuron differentiation

Motor neurons were differentiated from iPSCs following a previously published protocol.[12,13] Basic neural medium (BNM, 1:1 mixture of DMEM/F12 and Neurobasal, 0.5X N2, 0.5X B27, 0.5X GlutaMAX, 1X antibiotic-antimycotic, and 100 µM ascorbic acid) serves as the base medium for all other formulations used in this protocol. iPSCs were seeded on matrigel coated flasks in neural induction medium (BNM supplemented with 2 µM SB431542, 2 µM DMH1, 3 µM CHIR99021) with a full media change performed every other day. After 6 days, cells were passaged in patterning medium (BNM supplemented with 1 µM CHIR99021, 2 µM SB431542, 2 µM DMH1, 0.1 µM retinoic acid (RA) and 0.5 µM purmorphamine (PMN)) onto poly-L-ornithine- and laminin-coated flasks and cultured for a further 6 days with a full media change performed every other day. Cells were then passaged onto poly-L-ornithine- and laminin-coated flasks in expansion medium (BNM supplemented with 3 µM CHIR99021, 2 µM SB431542, 2 µM DMH1, 0.1 µM RA and 0.5 µM PMN, and 0.5 mM valproic acid (VPA)), with a full media change performed every other day for 6 days to obtain motor neural progenitor cells (M-NPCs). M-NPCs were dissociated as single cells and seeded onto poly-L-ornithine- and laminin-coated plates in final differentiation medium (BNM supplemented with 0.5 µM RA, 0.1 µM PMN, 0.1 µM Compound E (CpdE), 10 ng/mL insulin-like growth

factor-1 (IGF-1), brain-derived neurotrophic factor (BDNF), and ciliary neurotrophic factor (CNTF)), with a half media change once per week for final differentiation into motor neurons (MNs). MNs were considered mature and collected for western blotting after four weeks of differentiation.

Dopaminergic neuron differentiation

Dopaminergic neurons were differentiated from iPSCs following a protocol of floor-plate induction with additional modifications.[14,15] Briefly, iPSCs were dissociated into single cells to form embryoid bodies (EBs). EBs were grown on low-attachment plates for one week in DMEM/F12 supplemented with 1X N2 and 1X B27, in the presence of 10 µM SB431542, 200 ng/mL Noggin, 200 ng/mL sonic hedgehog, 3 µM CHIR99021 and 100 ng/mL Fibroblast growth factor 8 (FGF8). On day 7, EBs were transferred, in the same media, to poly-L-ornithine- and laminin-coated plates. On day 14, rosettes were selected semi–manually and cultured as a monolayer in DMEM/F12 supplemented with 1X N2 and 1X B27 on poly-L-ornithine- and laminin-coated plates to generate DA neural progenitor cells (DA-NPCs). DA-NPCs were passaged at a ratio of 1:3 every 5-7 days. DA-NPCs were then cultured in neurobasal medium, supplemented with 1X N2 and 1X B27, in the presence of 1 µg/mL laminin, 500 µM dibutyryl-cAMP (db-cAMP), 20 ng/mL BDNF, 20 ng/mL glial-derived neurotrophic factor (GDNF), 200 µM ascorbic acid, 100 nM CpdE and 1 ng/mL transforming growth factor β3 (TGF-β3), with a half media change twice per week for final differentiation into dopaminergic neurons. Dopaminergic neurons were considered mature and collected for western blotting after four weeks of differentiation.

Cortical neuron differentiation

Cortical neurons were differentiated from iPSCs following a published protocol.[16] Briefly, iPSCs were dissociated using gentle cell dissociation reagent and seeded in induction medium 1 (DMEM/F12 with Glutamax supplemented with 1X N2, 1X B27, 1X MEM Non Essential Amino Acids (NEAA), 1 µg/mL Laminin, 10 µM SB431542, 200 ng/mL Noggin, 0.1% bovine serum albumin (BSA)) on matrigel-coated 6-well plates with a full media change performed daily for one week. Cells were then cultured in induction medium 2 (DMEM/F12 with Glutamax supplemented with 1X N2, 1X B27, 1X NEAA, 1 µg/mL Laminin, 0.1% BSA) with a full media change performed daily, for a further five days. To generate neurospheres, cells were transferred to a suspension culture in expansion medium (DMEM/F12 with Glutamax, 1X N2, 1X B27, 1X NEAA, 1 µg/mL Laminin, 20 ng/mL epidermal growth factor (EGF), 20 ng/mL fibroblast growth factor basic (FGFb)), for two days. The resulting neurospheres were collected and replated in expansion medium as a monolayer on a matrigel-coated dish. A second identical purification was performed. The resulting cortical neural progenitor cells (C-NPCs) were further expanded in the same expansion medium on poly-L-ornithine- and laminin-coated flasks. The next day a half media change into STEMdiff™ Forebrain Neuron Differentiation Medium (STEMdiff™ Forebrain Neuron Differentiation Kit) was performed to begin differentiation to cortical neurons. C-NPCs were maintained in this media for one week with a half media change performed every other day. A half media change to STEMdiff™ Forebrain

Neuron Maturation Medium (STEMdiff™ Forebrain Neuron Maturation Kit) was then performed. Cortical neurons were maintained in this media for an additional 21 days with a half media change performed every other day until mature, at which point they were collected for western blotting.

Oligodendrocyte differentiation

Oligodendrocytes were differentiated from iPSCs following a recently published protocol.[17] The base media for all other formulations in this protocol is as follows: DMEM/F12 with Glutamax supplemented with 1X N2, 1X B27, 1X NEAA, 55 mM b-mercaptoethanol, 25 mg/mL Insulin, and 2 mg/mL heparin. First, iPSCs were directed toward a neural progenitor fate in base media supplemented with 10 µM SB31542 and 2 µM DMH1, with daily media change over eight days. Followed by patterning with 100 nM RA and 1 µg/mL PMN in base media with daily media change, for four days. Cells were then transferred from monolayer to suspension culture in the same medium for an additional eight days to form neurospheres. Oligodendrocyte precursor cells (OPCs) were then generated and expanded in suspension using OPC media (base media supplemented with 10 ng/mL PDGF-AA, 10 ng/mL IGF-1, 10 ng/mL NT-3, 5 ng/mL HGF, 60 ng/mL 3, 3′, 5-Triiodo-L-thyronine (T3), 100 ng/mL biotin, and 1 µM db-cAMP) for 10 days. Following this, the cells were plated in OPC media onto poly-L-ornithine/laminin-coated vessels with half media changes performed every other day to support further differentiation toward the OPC lineage, which continues until day 75. At this stage, cells were detached and passaged using TrypLE™ Express Enzyme. In the final differentiation step, cells were exposed to ScienCell Astrocyte Medium supplemented with ScienCell Astrocyte Growth Supplements (AGS) for 10 days. AGS was then withdrawn, and final maturation completed by reintroducing IGF-1 and T3 at the previously described concentrations for a further 10 days, with half media changes performed every other day. At this point, oligodendrocytes were considered mature and collected for western blotting.

Astrocyte differentiation

Astrocytes were differentiated from iPSCs following a previously published protocol.[18] First, iPSCs were differentiated into neural progenitor cells following the steps described above for the generation of M-NPCs. M-NPCs were dissociated as single cells and plated at a low cell density (15,000 cells/cm^2) onto a matrigel coated vessel in M-NPC expansion media (as described above). The next day, medium was replaced with Astrocyte Differentiation Medium (ScienCell Astrocyte Medium containing AGS, 1% fetal bovine serum (FBS) (ScienCell Research Laboratories), 1% penicillin streptomycin (Wisent Bioproducts)). Cells were passaged in the same media at a ratio of 1:2 once per week and were maintained under these culture conditions for 30 days, with a half media change performed every 3-4 days. FBS was then withdrawn to promote astrocyte maturation. Cells were maintained for an additional four weeks with a half media change performed twice per week prior to astrocyte collection for western blotting.

Microglia differentiation

iPSC-derived microglia were differentiated following a published protocol.[19] Briefly, iPSCs were differentiated to hematopoietic precursor cells (iHPCs) using the STEMCELL Technologies STEMdiff™ Hematopoietic Kit. iHPCs were harvested on days 10 and 12 of iHPC differentiation and seeded on matrigel-coated 6-well plates in microglia differentiation media (MDM, DMEM/F12 HEPES no phenol red supplemented with 2X Insulin-transferrin-selenite, 2X B27, 0.5X N2, 1X Glutamax, 1X NEAA, 400 µM monothioglycerol, and 5 µg/mL insulin) + three cytokine cocktail (25 ng/mL M-CSF, 100 ng/mL IL-34, and 50 ng/mL TGF-β1) for further differentiation into microglia. Cells were supplemented with MDM + three cytokine cocktail every other day, with a full media change performed on day 12, for 24 days of iMG differentiation. On day 25 a full media change to MDM + five cytokine cocktail (25 ng/mL M-CSF, 100 ng/mL IL-34, 50 ng/mL TGF-β1, 100 ng/mL CD200, and 100 ng/mL CX3CL1) was performed, followed by supplementation with MDM + five cytokine cocktail on day 27. Microglia were considered mature and utilized for downstream experiments after 28 days of microglial differentiation.

Microglia treatments

For bulk RNA sequencing experiments, iPSC-derived microglia were left untreated or treated with 20 ng/mL IFNγ for 24 hours. For western blotting experiments, iPSC-derived microglia were left untreated or treated for 24 hours with 20 ng/mL interferon γ (IFNγ) and 100 ng/mL lipopolysaccharide (LPS), or with 20 ng/mL IL-4. Fetal microglia were also treated for 24 hours with 20 ng/mL IFNγ and 100 ng/mL LPS or left untreated.

LI-COR Image Studio Lite software was used for band intensity quantifications. For each defined lane, a box was created around the band(s) corresponding to the protein of interest. The software calculates the signal by summing the pixel intensities within each box and subtracting the product of the background value and the area. Relative expression was then calculated by dividing the signal of IFNγ + LPS-treated iPSC microglia or IL-4 treated iPSC microglia by the signal from untreated cells. Similarly, the signal from IFNγ + LPS-treated fetal microglia was divided by the signal from untreated fetal microglia.

Human primary cell isolation and culture

Peripheral blood mononuclear cell-derived macrophages were generated as previously described.[20] Briefly, peripheral blood mononuclear cells were isolated from the venous blood using Ficoll-Paque density gradient centrifugation and monocytes were positively selected using $CD14^+$ immunomagnetic beads (Miltenyi Biotec). Monocytes were differentiated in RPMI-1640 supplemented with 10% fetal bovine serum (Wisent Bioproducts), 1% penicillin streptomycin (Thermo Fisher), 1% glutamine and recombinant 25 ng/mL M-CSF for 6 days. Macrophages were treated with IFNγ (48h) and 100 ng/mL LPS (last 24h) or with 20 ng/mL each interleukin-4 and interleukin-13 (48h).

Fetal microglia and astrocytes were isolated as previously described from second trimester fetal cerebrum tissues.[21,22] Tissues were obtained from the Birth Defects Research Laboratory, University of

Washington, Seattle, USA, with maternal written consent and under approval from local ethics boards. Briefly, tissues were minced with a scalpel, digested using trypsin and DNase and filtered, following which the isolated cells were grown on a poly-L-lysine coated flask in MEM with 5% fetal bovine serum (Wisent Bioproducts), 1% penicillin streptomycin (Thermo Fisher) and 1% glutamine. After 5-7 days, the floating microglia and the adherent astrocytes were harvested separately for downstream experiments.

Bulk RNA sequencing from iPSC-derived microglia

RNA extraction was performed using the Qiagen RNeasy kit (74106), quality control, library preparation and sequencing was performed by Genome Quebec (Montreal, Canada). Library preparation was carried out using an NEBNext RNA Library Prep kit (New England Biolabs) and samples were sequenced on an Illumina Novaseq 6000. Reads were aligned to the human reference genome GRCh38 using STAR aligner.[23] Count normalization and differential gene expression analysis was performed using DESeq2 using three technical replicates of iPSC-derived microglia differentiated and processed in parallel.[24] An FDR-adjusted p-value of ≤ 0.05 and log2 fold change of -/+ 0.5 were used to determine significantly differentially expressed genes (DEGs). K-means clustering was used to aggregate IFNγ DEGs, over-representation analysis (ORA) of these clusters was performed using WebGestalt.[25]

Key resources table

REAGENT or RESOURCE	SOURCE	IDENTIFIER
Antibodies		
Mouse monoclonal anti-ACSL5 (Clone 5H8) (Figures 3, 5 and S2)	Abnova	CAT#H00051703-M01; RRID:AB_509241
Rabbit recombinant monoclonal anti-ALS2 (clone EPR11185) (Figures 3, 5 and S2)	Abcam	CAT#ab170896; RRID:AB_2885099
Rabbit polyclonal anti-ANXA11 (Figures 3, 5 and S2)	Aviva Systems Biology	CAT#ARP87950_P050; RRID:AB_2894925
Rabbit recombinant monoclonal anti-ATXN2 (clone EPR23630-49) (Figures 3, 5 and S2)	Abcam	CAT#ab254362; RRID:AB_2885130
Mouse monoclonal anti-C9orf72 clone GT1553 (Figures 3, 5 and S2)	GeneTex	CAT#GTX634482; RRID:AB_2784545
Rabbit recombinant monoclonal anti-CAV1 (clone SZ02-01) (Figure 3)	Thermo Fisher Scientific	CAT#MA5-32020; RRID:AB_2809314
Rabbit recombinant monoclonal anti-CAV1 (Clone ARC50848) (Figure S2)	ABclonal	CAT#A19006; RRID:AB_2862498
Rabbit polyclonal anti-CHCHD10 (Figures 3 and 5)	GeneTex	CAT#25671-1-AP; RRID:AB_2880187
Mouse monoclonal anti-CHCHD10 (clone OTI3B8) (Figure S2)	Thermo Fisher Scientific	CAT#MA5-27535; RRID:AB_2724132
Rabbit recombinant monoclonal anti-CHMP2B (clone JE54-35) (Figures 3 and S2)	Thermo Fisher Scientific	CAT#MA5-36184; RRID:AB_2890433
Rabbit recombinant monoclonal anti-CHMP2B (clone EPR10807(B)) (Figure 5)	Abcam	CAT#ab157208; RRID:AB_2885096
Rabbit recombinant monoclonal anti-FIG4 (clone N202/7R) (Figures 3, 5 and S2)	Addgene	CAT#192037; RRID:AB_2916241
Mouse monoclonal anti-FUS (clone CL0190) (Figures 3, 5 and S2)	Abcam	CAT#ab154141; RRID:AB_2885092
Mouse monoclonal anti-HNRNPA1 (Clone 4B10) (Figures 3 and S2)	Bio-Techne (Novus Biologicals)	CAT#NB100-672; RRID:AB_524308
Mouse monoclonal anti-HNRNPA2B1 (clone DP3B3) (Figures 3 and S2)	Bio-Techne (Novus Biologicals)	CAT#NB120-6102; RRID:AB_790226
Rabbit recombinant monoclonal anti-LGALS1 (clone EPR3206(2)) (Figures 3 and S2)	Abcam	CAT#ab138513; RRID:AB_2894851
Rabbit recombinant monoclonal anti-MATR3 (clone EPR10634(B)) (Figures 3, 5 and S2)	Abcam	CAT#ab151739; RRID:AB_2885091
Rabbit polyclonal anti-NEK1 (Figures 3 and S2)	GeneTex	CAT#GTX130828; RRID:AB_2886357
Mouse monoclonal anti-OPTN (clone 6C1H4) (Figures 3, 5 and S2)	Proteintech	CAT#60293-1-Ig; RRID:AB_2881408
Rabbit recombinant monoclonal anti-PFN1 (clone ARC1469) (Figures 3, 5 and S2)	ABclonal	CAT#A9188; RRID:AB_2863682
Rabbit recombinant monoclonal anti-SIGMAR1 (Clone D4J2E) (Figures 3, 5 and S2)	Cell Signaling Technology	CAT#61994; RRID:AB_2799617
Rabbit recombinant monoclonal anti-SOD1 (Clone EP1727Y) (Figures 3 and 5)	Abcam	CAT#ab51254; RRID:AB_882757
Rabbit polyclonal anti-SOD1 (Figure S2)	GeneTex	CAT#GTX100554; RRID:AB_10618670
Rabbit recombinant monoclonal anti-SPG11 (clone 2H25L11) (Figures 3, 5 and S2)	Thermo Fisher Scientific	CAT#702776; RRID:AB_2725406
Rabbit recombinant monoclonal anti-SQSTM1 (clone EPR4844) (Figure 5 and S2)	Abcam	CAT#ab109012; RRID: AB_2810880
Mouse monoclonal anti-SQSTM1 (clone 2C11) (Figure 3)	Abcam	CAT#ab56416; RRID: AB_945626
Rabbit recombinant monoclonal anti-TAF15 (clone JE61-92) (Figure 3 and S2)	Thermo Fisher Scientific	CAT#MA5-44822; RRID: AB_2931279
Rabbit recombinant monoclonal anti-TARDBP (clone 11N20) (Figures 3, 5 and S2)	Proteintech	CAT#80001-1-RR; RRID: AB_2882933
Rabbit recombinant monoclonal anti-TBK1 (Clone EP611Y) (Figures 3 and 5)	Abcam	CAT#ab40676; RRID: AB_776632

Rabbit recombinant monoclonal anti-TBK1 (clone E8I3G) (Figure S2)	Cell Signaling Technology	CAT#38066; RRID: AB_2827657
Rabbit recombinant monoclonal anti-TIA1 (Clone D1Q3K) (Figures 3, 5 and S2)	Cell Signaling Technology	CAT#86050; RRID: AB_2800070
Rabbit recombinant monoclonal anti-TUBA4A (Clone EPR13478(B)) (Figures 3 and 5)	Abcam	CAT#ab176560; RRID: AB_2860019
Rabbit recombinant monoclonal anti-TUBA4A (Clone JM73-24) (Figure S2)	Thermo Fisher Scientific	CAT#MA5-32738; RRID: AB_2810015
Mouse monoclonal anti-UBQLN2 (clone 6H9) (Figures 3, 5 and S2)	Abcam	CAT#ab190283; RRID: AB_2747782
Rabbit recombinant monoclonal anti-VAPB (clone EPR27026-50) (Figures 3 and 5)	Abcam	CAT#ab315013; RRID:AB_3086770
Rabbit polyclonal anti-VAPB (Figure S2)	Thermo Fisher Scientific	CAT#PA5-53023; RRID:AB_2649391
Rabbit recombinant monoclonal anti-VCP (Clone 7F3) (Figures 3 and 5)	Cell Signaling Technology	CAT#2649; RRID:AB_2214629
Rabbit recombinant monoclonal anti-VCP (clone EPR3307(2)) (Figure S2)	Abcam	CAT#ab109240; RRID:AB_10862588
Chemicals, peptides, and recombinant proteins		
Astrocyte Growth Supplements (AGS)	ScienCell Research Laboratories	1852
Astrocyte Medium (AM)	ScienCell Research Laboratories	1801-b
Interferon γ (IFNγ)	Peprotech	CAT#300-02
Interleukin 4 (IL-4)	Peprotech	CAT#200-04
Lipopolysaccharide (LPS)	Thermo Fisher	CAT#00-4976-93
mTeSR1	STEMCELL Technologies	CAT#85850
STEMdiff™ Forebrain Neuron Differentiation Kit	STEMCELL Technologies	CAT#08600
STEMdiff™ Forebrain Neuron Maturation Kit	STEMCELL Technologies	CAT#08605
STEMdiff™ Hematopoietic Kit	STEMCELL Technologies	CAT#05310
STEMdiff™ Hematopoietic Kit	STEMCELL Technologies	CAT#05310
STEMdiff™ Hematopoietic Kit	STEMCELL Technologies	CAT#05310
Deposited data		
Supplementary Table 1_IFNG_DEG_analysis	doi.org/10.5281/zenodo.17116576	NA
Experimental models: Cell lines		
Healthy control iPSCs from the AIW002-02 background	EDDU, McGill University	NA
Healthy control iPSCs from the QPN929 background	EDDU, McGill University	NA
Software and algorithms		
LI-COR Image Studio Lite	licorbio.com/image-studio	NA
Other		
Antibody Registry	antibodyregistry.org	RRID:SCR_006397
Brain RNA-Seq; Human brain	brainrnaseq.org	RRID:SCR_013736
Cellosaurus - a knowledge resource on cell lines	cellosaurus.org	RRID:SCR_013869
Cellosaurus - a knowledge resource on cell lines	cellosaurus.org	RRID:SCR_013869
CiteAb - Reagent Search & Life Science Data	citeab.com	RRID:SCR_009653
DepMap: The Cancer Dependency Map Project at Broad Institute	depmap.org/portal	RRID:SCR_017655
PubMed	pubmed.ncbi.nlm.nih.gov	RRID:SCR_004846
The Allen Mouse Brain Atlas	mouse.brain-map.org/static/atlas	RRID:SCR_008848
The Human Protein Atlas	proteinatlas.org	RRID:SCR_006710

Table of lysates

Figure	Batch	Lysate	Cell type	Background
Figure 3	A	Motor neuron[a]	iPSC-derived mature motor neurons	AIW002-02
Figure 3	A	Cortical neuron[a]	iPSC-derived mature cortical neurons	AIW002-02
Figure 3	A	Dopamine neuron[a]	iPSC-derived mature dopamine neurons	AIW002-02
Figure 3	A	Oligodendrocyte[a]	iPSC-derived mature oligodendrocytes	AIW002-02
Figure 3	A	Astrocyte[a]	iPSC-derived mature astrocytes	AIW002-02
Figure 3	A	Microglia[a]	iPSC-derived mature microglia	AIW002-02
Figure 3	A	Fetal astrocyte[a]	Human fetal astrocytes from donor A (#322)	-
Figure 3	A	Fetal microglia[a]	Human fetal microglia	-
Figure 3	A	MDM[a1, a2]	Human monocyte-derived M0 macrophages from donors A1 or A2	-
Figure S2	B	Motor neuron[c]	iPSC-derived mature motor neurons	AIW002-02
Figure S2	B	Cortical neuron[b]	iPSC-derived mature cortical neurons	AIW002-02
Figure S2	B	Dopamine neuron[b]	iPSC-derived mature dopamine neurons	AIW002-02
Figure S2	B	Oligodendrocyte[b]	iPSC-derived mature oligodendrocytes	AIW002-02
Figure S2	B	Astrocyte[b]	iPSC-derived mature astrocytes	AIW002-02
Figure S2	B	Microglia[b]	iPSC-derived mature microglia	QPN929
Figure S2	B	Fetal astrocyte[b]	Human fetal astrocytes from donor B	-
Figure S2	A	Fetal microglia[a]	Human fetal microglia	-
Figure S2	B	MDM[b1, b2]	Human monocyte-derived M0 macrophages from donors B1 or B2	-
Figure 5	A	Motor neuron[a]	iPSC-derived mature motor neurons	AIW002-02
Figure 5	C	NT microglia[c]	iPSC-derived mature microglia untreated	AIW002-02
Figure 5	C	IFNγ + LPS microglia[c]	iPSC-derived mature microglia treated with IFNγ and LPS	AIW002-02

Figure 5	C	IL-4 microglia[c]	iPSC-derived mature microglia treated with IL-4	AIW002-02
Figure 5	C	NT fetal microglia[c]	Human fetal microglia untreated	-
Figure 5	C	IFNγ + LPS fetal microglia[c]	Human fetal microglia treated with IFNγ and LPS	-

Results

Genetic prioritization and initial characterization of ALS-RAP targets

We selected 33 ALS-related genes that met the criterion of well-replicated genetic inheritance: *ACSL5*, *ALS2*, *ANG*, *ANXA11*, *ATXN2*, *C9orf72*, *CAV1*, *CCNF*, *CHCHD10*, *CHMP2B*, *FIG4*, *FUS*, *HNRNPA1*, *HNRNPA2B1*, *KIF5A*, *LGALS1*, *MATR3*, *NEK1*, *OPTN*, *PFN1*, *SETX*, *SIGMAR1*, *SOD1*, *SPG11*, *SQSTM1*, *TAF15*, *TARDBP*, *TBK1*, *TIA1*, *TUBA4A*, *UBQLN2*, *VAPB*, *VCP*. Building on the 2024 classification by Nijs and Van Damme,[6] these genes were categorized into six groups based on variant frequency and estimated pathogenic impact: (1) rare variants with high effect size, (2) rare variants with intermediate effect size, (3) rare variants with small effect size, (4) rare variants with unknown effect size, (5) common variants with unknown effect size, and (6) common variants with small effect size (Table 1). To assess the degree of characterization, PubMed searches were performed for each gene using either the gene name alone or in combination with the term “ALS” (Table 1). The results, visualized as a line scan plot (Fig. 1A), revealed that *SOD1*, *TARDBP*, *C9orf72*, and *FUS* dominate the field, accounting for 10,809 of 13,173 total publications (>80%) in the context of ALS, with *FUS* contributing the fewest among these four (1,332). In contrast, the remaining 29 genes are far less studied in ALS and collectively define what we refer to as the dark ALS-ome, with *VCP* being the most cited among them (267 publications). Notably, seven genes—*VCP*, *OPTN*, *SQSTM1*, *TBK1*, *ANG*, *TIA1*, and *CAV1*—have attracted substantial attention in other biological contexts, with TIA1 contributing the fewest publications in this group (1,146). The remaining 21 genes are even less characterized, with each represented by fewer than 574 PubMed entries.

STRING analysis of the 33 ALS-related proteins revealed limited evidence of direct protein–protein interactions, with the exception of clusters among autophagy regulators (TBK1, OPTN, UBQLN2, SQSTM1) and RNA-binding proteins (TIA1, ATXN2, TARDBP, FUS, MATR3, HNRNPA1, and HNRNPA2B1) (Figure S1). This suggests that, while these gene products may converge on shared cellular mechanisms, they likely function through distinct molecular pathways, act in different cell types, or remain insufficiently characterized to fully define their roles.

To begin uncovering such potential patterns, we investigated cell-type-specific expression of the 33 ALS-associated genes using RNA sequencing data from the Human Protein Atlas (HPA), a publicly available repository integrating multiple omics datasets to map human gene expression across cells, tissues, and organs.[26] A heatmap was generated to compare RNA expression levels across neurological cell populations, with the aim of distinguishing neuron-enriched genes from those expressed in glial cells (Figure 1B). Notably, RNA sequencing data for motor neurons are not available in the HPA dataset. Five expression clusters were identified: astrocyte-enriched (*SQSTM1*); microglia-enriched (*ACSL5*, *ANXA11*, *C9orf72*, *FIG4*, *FUS*, *HNRNPA1*, *SETX*, and *TBK1*); neuron-enriched (*ALS2*, *CCNF*, *KIF5A*, and

TUBA4A); oligodendrocyte-enriched (*CAV1*, *CHMP2B*, *LGALS1*); and a group with low cell-type specificity or broad expression (*ATXN2*, *CHCHD10*, *HNRNPA2B1*, *NEK1*, *OPTN*, *PFN1*, *SOD1*, *SPG11*, *TAF15*, *TARDBP*, *UBQLN2*, *VAPB*, and *VCP*). Four genes were barely detected in neurological cell types (*ANG*, *MATR3*, *SIGMAR1*, and *TIA1*). Within all 33 ALS genes, *ACSL5*, *CCNF*, *TUBA4A* and *CAV1* showed significant expression in only a single cell type. Together, these findings suggest that ALS-associated genes are not uniformly neuron-centric but instead display diverse expression signatures across neuronal and glial lineages.

Tool generation for ALS-RAP associated proteins

To generate and validate research tools for the 33 ALS-RAP targets and to confirm the RNA expression patterns at the protein level, we leveraged the Antibody Characterization through Open Science (YCharOS) initiative to identify high-quality antibodies for ALS-RAP proteins at endogenous levels. YCharOS brings together leading antibody manufacturers and KO cell line providers who donate their reagents for systematic characterization. Antibodies are tested in side-by-side comparisons by western blot (WB), immunoprecipitation (IP), and immunofluorescence (IF) assays using standardized, industry-endorsed KO-based protocols.[27,28] The resulting KO-based characterization data are compiled into target-specific antibody characterization reports, which are rapidly deposited on Zenodo (zenodo.org/communities/ycharos), an open-access repository hosted by CERN, and subsequently submitted for peer-reviewed publication at *F1000Research* (f1000research.com/gateways/ycharos), to ensure PubMed indexing. These articles are gathered within the YCharOS Gateway, which includes a dedicated ALS section that hosts the ALS-RAP reports.

We first assessed the availability of renewable antibodies (monoclonal and recombinant) for all ALS-RAP targets using the CiteAb reagents database (citeab.com), as renewable formats ensure long-term supply, consistent and higher performance, and reduced reliance on animal immunization.[29] Moreover, renewable antibodies demonstrated at least equal, if not superior specificity compared with traditional hybridoma-derived or polyclonal antibodies.[30] Nine proteins—VCP, FUS, GLE1, UBQLN2, KIF5A, MATR3, ATXN2, OPTN, and PFN1—lacked commercial renewable antibodies. To address this gap, the Structural Genomics Consortium (SGC), an international public–private partnership dedicated to advancing our understanding of the human proteome, generated recombinant protein antigens and used animal-free phage-display technology to develop single-chain variable fragment (scFv) recombinant antibodies.[31] Antibody-encoding plasmids were deposited at Addgene, allowing researchers to produce these reagents independently. SGC-derived scFv antibodies were tested alongside commercial antibodies in our characterization pipeline.

In parallel, we assessed KO cell line coverage for the 33 ALS-RAP targets. Twenty-one KOs were available from YCharOS partners in commonly used cancer-derived lines, selected based on parental

expression levels above 3.0 $\log_2$(TPM+1) in the DepMap database—an expression threshold suitable for antibody characterization studies.[27] To complete coverage, 12 additional custom KO lines were generated and are available upon request, while *VCP* was targeted with siRNA as it is an essential gene. To enhance reagent traceability and reuse, we obtained Research Resource Identifiers (RRIDs) for all antibodies tested and KO cell lines used from the Antibody Registry and Cellosaurus databases,[32,33] which are cited in the corresponding antibody characterization reports (Table 1).

Antibody performance and coverage for ALS-RAP proteins

We characterized 296 antibodies—comprising 288 commercially available reagents and 8 custom scFv antibodies—targeting 33 ALS-associated proteins. For 26 targets, antibodies were tested across WB, IP and IF. Six proteins—ANG, CAV1, CCNF, KIF5A, SETX and LGALS1—were tested only in WB due to specific limitations: specialized cell treatments (e.g., cell cycle arrest for CCNF), lack of manufacturer recommendations for IP or IF (SETX, CAV1, LGALS1, ANG), or undetectable expression in culture cell lines (KIF5A). Antibodies against the secreted protein ANG were tested in WB and IP only. For each protein, a comprehensive validation report was compiled, reviewed in collaboration with YCharOS industry partners, and published on Zenodo, with some also appearing in *F1000Research*, as described in the previous results section (Figure 2A and Table 1). Specific and renewable antibodies were identified for most targets across multiple applications (Figure 2A), indicating that high-quality reagents already exist for many disease-associated proteins, including understudied ones such as ACSL5 (only 4 ALS-related citations and 192 PubMed entries in total). Although YCharOS characterization reports do not assign performance scores, the antibodies used in this study were chosen based on these data, with a focus on renewable and selective reagents. All catalogue numbers are listed in the “Key Resources Table”.

CiteAb.com searches revealed that among the 64 top- and second-most-cited antibodies across 32 ALS-RAP targets (data unavailable for TUBA4A), 40 were polyclonal and 24 were renewable (Figure 2B). The polyclonals accounted for 7,124 literature citations, compared with 1,205 for the renewable antibodies (Figure 2C), underscoring the continued reliance on polyclonals and the need for renewable alternatives. Across all targets, at least one renewable KO-validated antibody was identified in WB, IP, and IF for 94%, 73%, and 64% of the ALS proteins, respectively. For targets without renewable antibody coverage, KO-validated polyclonal antibodies were available in 3% (WB), 12% (IP), and 8% (IF) of cases (Figure 2D). Overall, 254 of 296 antibodies detected their intended target in WB, 95 of 244 successfully immunoprecipitated their target, and 121 of 241 correctly localized their target in IF (Figure 2E). The newly developed scFv antibodies filled key gaps; for example, the scFv against PFN1 was the only antibody—among 18 tested—capable of immunoprecipitating the protein.[34] In contrast, no specific antibody has yet been identified for KIF5A, possibly reflecting either absent expression in the culture lines tested or insufficient specificity of existing antibodies. Collectively, these results demonstrate that

renewable, KO-validated antibodies cover most ALS-associated proteins, enabling reproducible studies of ALS biology.

Neurological expression scan of 29 ALS-RAP proteins

To explore connections between the ALS risk genes, we investigated protein expression patterns across neurological cell types. We differentiated human iPSCs into a range of neurons and glial cells, followed by WB analysis using identified KO-validated antibodies, prioritizing renewable antibodies. We selected iPSC-derived cells since they offer reproducible and relatively homogeneous differentiated cell populations for studying neurological cell types. Specifically, we generated lysates from iPSC-derived motor neurons, dopaminergic neurons, cortical neurons, astrocytes, oligodendrocytes and microglia following established protocols (see Material and Methods); most differentiated from the same healthy control iPSC line. However, differentiation protocols and donor genetic backgrounds can influence gene expression. To address this, we complemented our iPSC-based analyses with human primary cells—we isolated human fetal astrocytes, fetal microglia, and monocyte-derived macrophages (MDM). Proteins showing predominant expression in microglia and macrophages are referred to as myeloid-enriched.

We profiled 29 ALS-RAP proteins, with each assessed in two independent sources of the same cell types (Figure 3 and Figure S2). Four targets were excluded: CCNF, which requires cell-cycle blockade for detection; ANG, which is secreted and could not be detectable in cell lysates; KIF5A, for which no high-quality antibody was identified; and SETX, whose signal-to-noise ratio was too weak for reliable interpretation. Expression patterns, presented in alphabetical order, revealed the following:

ALS protein	Expression pattern
ACSL5	Predominant in myeloid cells
ALS2	Strong in all neuronal types and fetal astrocytes
ANXA11	Predominant in glial cells, particularly myeloid cells – weaker expression in neurons
ATXN2	Robust across all neuronal types with milder astrocytic expression
C9orf72	Predominant in myeloid cells with weaker expression in other cell types – barely detected in astrocytes
CAV1	Strong in astrocytes with weaker expression in oligodendrocytes
CHCHD10	High in iPSC-derived microglia, fetal microglia, and MDMs – moderate in neurons and absent in astrocytes
CHMP2B	Broad expression across all cell types
FIG4	Abundant in myeloid cells, weaker in neurons, and lowest in astrocytes
FUS	Detected across all cell types – enriched in neurons
HNRNPA1	High in neurons, oligodendrocytes, and astrocytes – low in myeloid cells
HNRNPA2B1	High in neurons, oligodendrocytes, and astrocytes – low in myeloid cells
LGALS1	Largely restricted to glial cells, also detectable in cortical neurons, but barely present in motor and dopaminergic neurons
MATR3	Broadly expressed though only mildly in myeloid cells
NEK1	Detected in neurons, oligodendrocytes, and astrocytes with minimal levels in myeloid cells

OPTN	Detected across all cell types at comparable levels
PFN1	Enriched in glial cells, particularly myeloid cells
SIGMAR1	Broad expression in all cell types, highest levels in cortical neurons and iPSC-derived astrocytes, lowest in myeloid cells
SOD1	Broadly detected with relatively uniform levels – lower abundance in myeloid cells
SPG11	Most abundant in glial cells – weaker expression in motor and dopaminergic neurons
SQSTM1	Detected across all cell types – enriched in myeloid cells and motor neurons
TAF15	Broadly expressed – enriched in astrocytes
TARDBP	Expressed across all cell types – enriched in neurons and astrocytes
TBK1	Broadly expressed – highest in fetal microglia and macrophages
TIA1	Expressed across cell types – barely detected in myeloid cells
TUBA4A	Primarily in neurons with additional expression in glial cells but minimal levels in microglia
UBQLN2	Present across all cell types – lowest in myeloid cells
VAPB	Primarily in neurons with additional expression in all glial cells
VCP	Detected at comparable levels across all cell types

Taken together, these results highlight distinct expression patterns across the ALS-RAP protein set. A subset of proteins showed preferential neuronal enrichment (ALS2, ATXN2, FUS, HNRNPA1, HNRNPA2B1, SIGMAR1, TARDBP, TUBA4A), whereas others were most abundant in glial populations, including astrocytes (ANXA11, SPG11, TAF15, CAV1) or myeloid cells (ACSL5, C9orf72, CHCHD10, FIG4, LGALS1, PFN1, SQSTM1, TBK1). Several proteins were broadly and uniformly expressed across cell types (CHMP2B, MATR3, NEK1, OPTN, SOD1, TIA1, UBQLN2, VCP, VAPB), while others showed more distinctive patterns, such as SQSTM1 (high in myeloid cells and motor neurons), and TBK1 (peaking in fetal microglia and macrophages).

Protein-level analyses confirmed several of the transcriptomic trends observed from our analysis of HPA sequencing data but also revealed important divergences. For example, ACSL5, C9orf72, ANXA11, FIG4, and TBK1 were enriched in myeloid cells at both RNA and protein levels, strengthening evidence for their microglial relevance. Conversely, FUS and HNRNPA1 were predicted by RNA profiling to be microglia-enriched, yet protein-level analysis revealed predominant expression across neuronal populations. Several broadly expressed genes at the RNA level showed cell type–specific differences in protein abundance – in particular CHCHD10, PFN1, SPG11, and SQSTM1 showed increased protein levels in myeloid populations while TARDBP and VAPB showed increased levels in neurons. In contrast, MATR3, SIGMAR1, and TIA1, which appeared nearly absent at the RNA level, were readily detectable as proteins in multiple cell types. Collectively, these comparisons underscore that RNA abundance is only ~33% predictive of protein expression,[35] highlighting the importance of direct protein-level validation. Together, the RNA–protein comparison demonstrates that ALS-associated proteins exhibit diverse and cell type–specific expression patterns, many of which are not apparent from transcriptomic data alone. In

particular, the enrichment of multiple ALS proteins in microglia and other glial populations suggests that non-neuronal cell types may contribute more directly to ALS pathogenesis than previously appreciated.

Ten ALS-associated proteins are regulated upon inflammatory stimulus

Immune-related mechanisms are increasingly recognized in ALS pathology.[36] For example, *C9orf72* KO mice show reduced viability following immune challenge.[37] Additionally, *C9orf72*-deficient microglia have been shown to display dysregulated response to LPS stimulation and altered inflammatory cytokine profiles.[38] Similarly, mutations in *SETX* have been linked to expanded activated $CD8^+$ T cells detected in spinal cord,[39] and recent work identified $CD4^+$ T cells reactive to C9orf72-derived peptides.[40] These findings suggest that immune activation and antigen presentation are important contributors to ALS-related neurodegeneration and that ALS-related genes could play significant roles in immune regulation.

Microglia and macrophages exhibit remarkable plasticity, adopting a wide range of dynamic functional states in response to many intrinsic and extrinsic factors: including sex, age, spatial location, and environmental cues. Although simplistic compared to the often-layered cues determining microglial and macrophages states *in vivo*, exposure to various cytokines and/or pathogen-associated molecular patterns (PAMPs) can influence the functional state of these cells *in vitro*. Here we use exposure to interferon-gamma (IFNγ) alone or in combination with lipopolysaccharide (LPS),[41] cues known to promote the release of pro-inflammatory cytokines and antimicrobial mediators, to model a pro-inflammatory state. Exposure to interleukin-4 (IL-4), which supports tissue repair, angiogenesis, and the resolution of inflammation,[42,43] was used to model an anti-inflammatory state.

Given the glial expression of many ALS-associated genes, we investigated whether inflammatory stimuli influence the expression of ALS-RAP targets at both the RNA and protein level. Bulk RNA sequencing was performed on unstimulated and IFNγ-stimulated iPSC-derived microglia. Transcriptome profiling confirmed a robust IFNγ response: ~50% of detected genes were differentially expressed, with roughly half (~25% of all genes) significantly upregulated and the other half (~25%) downregulated. Using k-means clustering, genes significantly differentially expressed in response to IFNγ were broadly grouped into three clusters based on their expression (normalized counts) (Figure 4A). Gene ontology over representation analysis revealed significant enrichment for innate immune response pathways in clusters of genes that are upregulated (clusters 1 and 3) in response to IFNγ, and significant enrichment for cell cycle pathways in the downregulated cluster 2 (Figure 4A, B). Additionally, many known IFNγ-responsive genes[41,44-48] are observed to be significantly differentially expressed in iPSC-derived microglia (Figure 4C). Full results of the differential gene expression analysis are presented in Supplementary Table 1. Among the 33 ALS-RAP genes, two (*CAV1* and *KIF5A*) were not detected, six (*ACSL5*, *C9orf72*, *NEK1*, *OPTN*, *TBK1*, and *TUBA4A*) were significantly upregulated, while *ATXN2*, *CCNF*, and *LGALS1* were significantly downregulated upon stimulation of iPSC-derived microglia with IFNγ (Fig. 4D).

To determine whether these transcriptional changes were reflected at the protein level, we performed immunoblotting of both iPSC-derived microglia and human fetal microglia stimulated with IFNγ and LPS, or left unstimulated, in addition to iPSC-derived microglia stimulated with IL-4 (Figure 5). A total of 23 proteins were examined, including genes with differential RNA expression and those with primary or broad myeloid expression. Proteins with minimal myeloid expression were excluded. Upon IFNγ and LPS stimulation, the mean fold-change—calculated from ratios in both iPSC- and fetal-derived microglia—was 1.5 or over for ACSL5, C9orf72, MATR3, OPTN, SQSTM1, TIA1, TUBA4A, UBQLN2, and VAPB. TBK1 showed an increase of 1.4-fold. Interestingly, CHCHD10 exhibited a marked 2.9-fold decrease in protein levels despite unchanged RNA levels, suggesting post-transcriptional or post-translational regulation.

Comparison of RNA and protein profiles revealed partial concordance. Five proteins—ACSL5, C9orf72, OPTN, TBK1, and TUBA4A—showed consistent upregulation at both RNA and protein levels. Conversely, the RNA-predicted decreases in LGALS1 and ATXN2 were not observed at the protein level. Additional proteins, including MATR3, SQSTM1, TIA1, UBQLN2, and VAPB, showed increased protein expression without corresponding RNA changes, highlighting the complexity of post-transcriptional regulation in microglia.

Discussion

Understanding the cell type–specific expression of disease-associated proteins is essential for uncovering pathogenic mechanisms and identifying therapeutic targets. Although the field increasingly recognizes the contribution of glial and immune mechanisms in ALS, motor neurons have remained the focus of most mechanistic studies. While RNA sequencing has greatly advanced our ability to infer expression patterns in neurodegenerative diseases, RNA abundance does not always correlate with protein levels, and proteomic validation is required. Using KO-validated renewable antibodies, we systematically profiled the expression of 29 ALS-associated proteins across iPSC-derived and primary neural cell types and compared these patterns with RNA data from the HPA. Both RNA and protein analyses consistently revealed that ALS-associated proteins are not predominantly neuronal but are also expressed in glial populations. Fifteen proteins showed concordance between RNA and protein, including five enriched in microglia (ACSL5, ANXA11, C9orf72, FIG4, and TBK1). In contrast, 18 proteins displayed discordant or divergent RNA–protein profiles. These findings highlight the importance of direct protein-level validation to complement transcriptomic predictions and to enhance the biological relevance of ALS disease models.

The majority of ALS-linked proteins remain part of the “dark ALS-ome,” with limited protein-level characterization despite strong genetic evidence. STRING analysis similarly revealed sparse connectivity among ALS proteins. Notably, we identified ten proteins whose levels change in microglia upon pro-inflammatory stimulation, underscoring the central role of immune signaling in ALS and suggesting a potential network of proteins that may act within a shared signaling pathway. Several of these converge on autophagy and proteostasis mechanisms. C9orf72, in complex with SMCR8 and WDR41,[49] regulates the initiation of autophagy,[50] with SMCR8 being phosphorylated directly by TBK1.[49] TBK1 also phosphorylates the autophagy receptors OPTN[51] and SQSTM1,[52] enhancing their cargo recruitment functions. UBQLN2 links the ubiquitin-proteasome system with autophagy,[53] TIA1 regulates autophagy regulator expression,[54] and VAPB at ER–mitochondria contact sites contributes to autophagosome biogenesis.[55] Moreover, C9orf72 was found to be predominantly expressed in microglia, suggesting that microglia could serve as the antigen-presenting cells in the CNS that drive the activation of $CD4^+$ T cells recently reported to recognize C9orf72-derived peptides.[40] Together, these proteins connect vesicle trafficking, stress response, and ubiquitin signaling to selective autophagy, highlighting a shared pathogenic axis in ALS.

This study has several limitations. First, we relied on iPSC-derived neurological cell types, which capture a tractable but restricted developmental and transcriptional state within specific genetic backgrounds. Protein absence in these models should be interpreted cautiously, as expression profiles may not reflect fully mature cells *in vivo*, and differentiation protocols can vary in efficiency across

laboratories. Complementary studies using KO-validated antibodies in immunohistochemistry across developmental stages and in postmortem human tissue will be essential to validate and extend our findings. Second, our RNA and protein analyses of iPSC-derived microglia used distinct polarization conditions (RNA after IFNγ alone; protein after IFNγ + LPS), limiting direct comparability, though regulation of key proteins was concordant across datasets. Third, our RNA analysis of the HPA dataset relied on arbitrary cutoff values to define enrichment. Fourth, the antibodies used did not target post-translational modifications (PTMs), though clear PTM-dependent regulation was observed (e.g., SQSTM1 upon IFNγ and LPS stimulation). Protein expression comparisons between iPSC-derived and primary cells also warrant careful interpretation. For example, ACSL5 is robustly expressed in fetal microglia but weaker in iPSC-derived microglia, whereas TARDP shows the opposite pattern. Such discrepancies likely reflect differences in developmental stage, culture conditions, and reprogramming artifacts rather than contradictions in biology.

While we identified high-quality renewable antibodies for most ALS-associated proteins, important gaps remain. For example, no suitable antibodies were found for KIF5A in this study, although newly available recombinant reagents and KO lines from YCharOS partners should allow this target to be revisited. Polyclonal antibodies are still the most commonly used reagents for ALS-associated proteins; however, we identified renewable, KO-validated alternatives for the majority of targets. In doing so, this work provides the field with a curated resource of best-performing antibodies to support reproducible studies of ALS biology. Leveraging this resource, we investigated ALS-associated proteins across neural cell types at the protein level, revealing microglia-enriched and immune-regulated proteins that highlight the critical contribution of glial biology to ALS and provide a foundation for refining disease models.

Acknowledgements

We would like to thank Kathleen Southern for the coordination of information exchange between laboratories involved in the ALS-RAP project. We would like to thank Abcam, ABCD Antibodies, ABclonal, Aviva System Biology, Cell Signaling Technology, Developmental Studies Hybridoma Bank, GeneTex, Revvity, Institute for Protein Innovation, MilliporeSigma, Novus Biologicals, Proteintech, R&D Systems, Thermo Fisher Scientific for providing antibodies and/or KO cell lines, free of charge, for ALS-RAP related targets. We would like to acknowledge the Birth Defects Research Laboratory, University of Washington, Seattle, USA for providing fetal tissues.

Grant Information

This work was supported by a grant from the Motor Neurone Disease Association, the ALS Association and ALS Canada to develop the ALS-Reproducibility Antibody Platform. This work was also supported by the Government of Canada through Genome Canada, Genome Quebec and Ontario Genomics (OGI-210) and by grant from the Quebec Consortium for Drug Discovery (CQDM), a grant from the Ministère de l'Économie, de l'Innovation et de l'Énergie du Québec. The Structural Genomics Consortium is a registered charity (no. 1097737) that receives funds from Bayer, Boehringer Ingelheim, Bristol Myers Squibb, Genentech, Genome Canada through Ontario Genomics Institute (grant no. OGI-196), the European Union (EU) and European Federation of Pharmaceutical Industries and Associations through the Innovative Medicines Initiative 2 Joint Undertaking (EUbOPEN grant no. 875510), Janssen, Merck (also known as EMD in Canada and the USA), Pfizer and Takeda. R.A. is supported by a Mitacs postdoctoral fellowship. This work was supported by a CIHR project grant (PJT-195804). E.A.F. is supported by a Canada Research Chair (Tier 1) in Parkinson's disease. J.P.R. is supported by an ALS Scholars in Therapeutics postdoctoral fellowship from the Sean M. Healey & AMG Center for ALS at Massachusetts General Hospital (MGH), ALS FindingACure, and FightMND. J.P.R. is supported by an ALS Scholars in Therapeutics postdoctoral fellowship from the Sean M. Healey & AMG Center for ALS at Massachusetts General Hospital (MGH), ALS FindingACure, and FightMND.

Competing Interests

The authors report no competing interests.

References

1. Leonard HL, Global Parkinson's Genetics P. Novel Parkinson's Disease Genetic Risk Factors Within and Across European Populations. *medRxiv*. Mar 17 2025;doi:10.1101/2025.03.14.24319455

2. Kim JJ, Vitale D, Otani DV, et al. Multi-ancestry genome-wide association meta-analysis of Parkinson's disease. *Nat Genet*. Jan 2024;56(1):27-36. doi:10.1038/s41588-023-01584-8

3. Bellenguez C, Kucukali F, Jansen IE, et al. New insights into the genetic etiology of Alzheimer's disease and related dementias. *Nat Genet*. Apr 2022;54(4):412-436. doi:10.1038/s41588-022-01024-z

4. Zhang J, Wang Y, Zhang Y, Yao J. Genome-wide association study in Alzheimer's disease: a bibliometric and visualization analysis. *Front Aging Neurosci*. 2023;15:1290657. doi:10.3389/fnagi.2023.1290657

5. van Rheenen W, van der Spek RAA, Bakker MK, et al. Common and rare variant association analyses in amyotrophic lateral sclerosis identify 15 risk loci with distinct genetic architectures and neuron-specific biology. *Nat Genet*. Dec 2021;53(12):1636-1648. doi:10.1038/s41588-021-00973-1

6. Nijs M, Van Damme P. The genetics of amyotrophic lateral sclerosis. *Curr Opin Neurol*. Oct 1 2024;37(5):560-569. doi:10.1097/WCO.0000000000001294

7. McKeever PM, Sababi AM, Sharma R, et al. Single-nucleus transcriptome atlas of orbitofrontal cortex in ALS with a deep learning-based decoding of alternative polyadenylation mechanisms. *Cell Genom*. Sep 17 2025:101007. doi:10.1016/j.xgen.2025.101007

8. Upadhya SR, Ryan CJ. Experimental reproducibility limits the correlation between mRNA and protein abundances in tumor proteomic profiles. *Cell Rep Methods*. Sep 19 2022;2(9):100288. doi:10.1016/j.crmeth.2022.100288

9. Tasaki S, Xu J, Avey DR, et al. Inferring protein expression changes from mRNA in Alzheimer's dementia using deep neural networks. *Nat Commun*. Feb 3 2022;13(1):655. doi:10.1038/s41467-022-28280-1

10. Liu Y, Beyer A, Aebersold R. On the Dependency of Cellular Protein Levels on mRNA Abundance. *Cell*. Apr 21 2016;165(3):535-50. doi:10.1016/j.cell.2016.03.014

11. Siletti K, Hodge R, Mossi Albiach A, et al. Transcriptomic diversity of cell types across the adult human brain. *Science*. Oct 13 2023;382(6667):eadd7046. doi:10.1126/science.add7046

12. Deneault E, Chaineau M, Nicouleau M, et al. A streamlined CRISPR workflow to introduce mutations and generate isogenic iPSCs for modeling amyotrophic lateral sclerosis. *Methods*. Jul 2022;203:297-310. doi:10.1016/j.ymeth.2021.09.002

13. Lepine S, Nauleau-Javaudin A, Deneault E, et al. Homozygous ALS-linked mutations in TARDBP/TDP-43 lead to hypoactivity and synaptic abnormalities in human iPSC-derived motor neurons. *iScience*. Mar 15 2024;27(3):109166. doi:10.1016/j.isci.2024.109166

14. Kriks S, Shim JW, Piao J, et al. Dopamine neurons derived from human ES cells efficiently engraft in animal models of Parkinson's disease. *Nature*. Nov 6 2011;480(7378):547-51. doi:10.1038/nature10648

15. C XQC, Deneault E, Abdian N, et al. Generation of patient-derived pluripotent stem cell-lines and CRISPR modified isogenic controls with mutations in the Parkinson's associated GBA gene. *Stem Cell Res*. Oct 2022;64:102919. doi:10.1016/j.scr.2022.102919

16. Maussion G, Rocha C, Abdian N, et al. Transcriptional Dysregulation and Impaired Neuronal Activity in FMR1 Knock-Out and Fragile X Patients' iPSC-Derived Models. *Int J Mol Sci*. Oct 5 2023;24(19)doi:10.3390/ijms241914926

17. Piscopo VEC, Chapleau A, Blaszczyk GJ, et al. The use of a SOX10 reporter toward ameliorating oligodendrocyte lineage differentiation from human induced pluripotent stem cells. *Glia*. Jun 2024;72(6):1165-1182. doi:10.1002/glia.24524

18. Soubannier V, Chaineau M, Gursu L, et al. Rapid Generation of Ventral Spinal Cord-like Astrocytes from Human iPSCs for Modeling Non-Cell Autonomous Mechanisms of Lower Motor Neuron Disease. *Cells*. Jan 24 2022;11(3)doi:10.3390/cells11030399

19. McQuade A, Coburn M, Tu CH, Hasselmann J, Davtyan H, Blurton-Jones M. Development and validation of a simplified method to generate human microglia from pluripotent stem cells. *Mol Neurodegener*. Dec 22 2018;13(1):67. doi:10.1186/s13024-018-0297-x

20. Healy LM, Jang JH, Won SY, et al. MerTK-mediated regulation of myelin phagocytosis by macrophages generated from patients with MS. *Neurol Neuroimmunol Neuroinflamm*. Nov 2017;4(6):e402. doi:10.1212/NXI.0000000000000402

21. Durafourt BA, Moore CS, Blain M, Antel JP. Isolating, culturing, and polarizing primary human adult and fetal microglia. *Methods Mol Biol*. 2013;1041:199-211. doi:10.1007/978-1-62703-520-0_19

22. Kieran NW, Suresh R, Dorion MF, et al. MicroRNA-210 regulates the metabolic and inflammatory status of primary human astrocytes. *J Neuroinflammation*. Jan 6 2022;19(1):10. doi:10.1186/s12974-021-02373-y

23. Dobin A, Davis CA, Schlesinger F, et al. STAR: ultrafast universal RNA-seq aligner. *Bioinformatics*. Jan 1 2013;29(1):15-21. doi:10.1093/bioinformatics/bts635

24. Love MI, Huber W, Anders S. Moderated estimation of fold change and dispersion for RNA-seq data with DESeq2. *Genome Biol*. 2014;15(12):550. doi:10.1186/s13059-014-0550-8

25. Elizarraras JM, Liao Y, Shi Z, Zhu Q, Pico AR, Zhang B. WebGestalt 2024: faster gene set analysis and new support for metabolomics and multi-omics. *Nucleic Acids Res*. Jul 5 2024;52(W1):W415-W421. doi:10.1093/nar/gkae456

26. Karlsson M, Zhang C, Mear L, et al. A single-cell type transcriptomics map of human tissues. *Sci Adv*. Jul 2021;7(31)doi:10.1126/sciadv.abh2169

27. Ayoubi R, Ryan J, Gonzalez Bolivar S, et al. A consensus platform for antibody characterization. *Nat Protoc*. Dec 17 2024;doi:10.1038/s41596-024-01095-8

28. Monteiro FL, Voskuil JLA, Williams C. YCharOS protocol for antibody validation. *Nat Protoc*. Jun 2025;20(6):1389-1390. doi:10.1038/s41596-024-01108-6

29. Marx V. Change-makers bring on recombinant antibodies. *Nat Methods*. Aug 2020;17(8):763-766. doi:10.1038/s41592-020-0915-8

30. Ayoubi R, Ryan J, Biddle MS, et al. Scaling of an antibody validation procedure enables quantification of antibody performance in major research applications. *Elife*. Nov 23 2023;12doi:10.7554/eLife.91645

31. Hornsby M, Paduch M, Miersch S, et al. A High Through-put Platform for Recombinant Antibodies to Folded Proteins. *Mol Cell Proteomics*. Oct 2015;14(10):2833-47. doi:10.1074/mcp.O115.052209

32. Bandrowski A, Pairish M, Eckmann P, Grethe J, Martone ME. The Antibody Registry: ten years of registering antibodies. *Nucleic Acids Res*. Jan 6 2023;51(D1):D358-D367. doi:10.1093/nar/gkac927

33. Bairoch A. The Cellosaurus, a Cell-Line Knowledge Resource. *J Biomol Tech*. Jul 2018;29(2):25-38. doi:10.7171/jbt.18-2902-002

34. Ayoubi R, McDowell I, Fotouhi M, et al. The identification of high-performing antibodies for Profilin-1 for use in Western blot, immunoprecipitation and immunofluorescence. *F1000Res*. 2023;12:348. doi:10.12688/f1000research.132249.1

35. Gry M, Rimini R, Stromberg S, et al. Correlations between RNA and protein expression profiles in 23 human cell lines. *BMC Genomics*. Aug 7 2009;10:365. doi:10.1186/1471-2164-10-365

36. Beers DR, Appel SH. Immune dysregulation in amyotrophic lateral sclerosis: mechanisms and emerging therapies. *Lancet Neurol*. Feb 2019;18(2):211-220. doi:10.1016/S1474-4422(18)30394-6

37. Burberry A, Wells MF, Limone F, et al. C9orf72 suppresses systemic and neural inflammation induced by gut bacteria. *Nature*. Jun 2020;582(7810):89-94. doi:10.1038/s41586-020-2288-7

38. Gao Y, Brothwood JL, Saini H, et al. Altered Inflammatory Signature in a C9ORF72-ALS iPSC-Derived Motor Neuron and Microglia Coculture Model. *Glia*. Sep 15 2025;doi:10.1002/glia.70084

39. Campisi L, Chizari S, Ho JSY, et al. Clonally expanded CD8 T cells characterize amyotrophic lateral sclerosis-4. *Nature*. Jun 2022;606(7916):945-952. doi:10.1038/s41586-022-04844-5

40. Michaelis T, Lindestam Arlehamn CS, Johansson E, et al. Autoimmune response to C9orf72 protein in amyotrophic lateral sclerosis. *Nature*. Oct 1 2025;doi:10.1038/s41586-025-09588-6

41. Kann O, Almouhanna F, Chausse B. Interferon gamma: a master cytokine in microglia-mediated neural network dysfunction and neurodegeneration. *Trends Neurosci*. Dec 2022;45(12):913-927. doi:10.1016/j.tins.2022.10.007

42. Quarta A, Berneman Z, Ponsaerts P. Neuroprotective modulation of microglia effector functions following priming with interleukin 4 and 13: current limitations in understanding their mode-of-action. *Brain Behav Immun*. Aug 2020;88:856-866. doi:10.1016/j.bbi.2020.03.023

43. Lambert C, Desbarats J, Arbour N, et al. Dendritic cell differentiation signals induce anti-inflammatory properties in human adult microglia. *J Immunol*. Dec 15 2008;181(12):8288-97. doi:10.4049/jimmunol.181.12.8288

44. Der SD, Zhou A, Williams BR, Silverman RH. Identification of genes differentially regulated by interferon alpha, beta, or gamma using oligonucleotide arrays. *Proc Natl Acad Sci U S A*. Dec 22 1998;95(26):15623-8. doi:10.1073/pnas.95.26.15623

45. Panagiotakopoulou V, Ivanyuk D, De Cicco S, et al. Interferon-gamma signaling synergizes with LRRK2 in neurons and microglia derived from human induced pluripotent stem cells. *Nat Commun*. Oct 14 2020;11(1):5163. doi:10.1038/s41467-020-18755-4

46. Hu X, Chakravarty SD, Ivashkiv LB. Regulation of interferon and Toll-like receptor signaling during macrophage activation by opposing feedforward and feedback inhibition mechanisms. *Immunol Rev*. Dec 2008;226:41-56. doi:10.1111/j.1600-065X.2008.00707.x

47. Ivashkiv LB. IFNgamma: signalling, epigenetics and roles in immunity, metabolism, disease and cancer immunotherapy. *Nat Rev Immunol*. Sep 2018;18(9):545-558. doi:10.1038/s41577-018-0029-z

48. Kang K, Bachu M, Park SH, et al. IFN-gamma selectively suppresses a subset of TLR4-activated genes and enhancers to potentiate macrophage activation. *Nat Commun*. Jul 25 2019;10(1):3320. doi:10.1038/s41467-019-11147-3

49. Sellier C, Campanari ML, Julie Corbier C, et al. Loss of C9ORF72 impairs autophagy and synergizes with polyQ Ataxin-2 to induce motor neuron dysfunction and cell death. *EMBO J*. Jun 15 2016;35(12):1276-97. doi:10.15252/embj.201593350

50. Yang M, Liang C, Swaminathan K, et al. A C9ORF72/SMCR8-containing complex regulates ULK1 and plays a dual role in autophagy. *Sci Adv*. Sep 2016;2(9):e1601167. doi:10.1126/sciadv.1601167

51. Wild P, Farhan H, McEwan DG, et al. Phosphorylation of the autophagy receptor optineurin restricts Salmonella growth. *Science*. Jul 8 2011;333(6039):228-33. doi:10.1126/science.1205405

52. Pilli M, Arko-Mensah J, Ponpuak M, et al. TBK-1 promotes autophagy-mediated antimicrobial defense by controlling autophagosome maturation. *Immunity*. Aug 24 2012;37(2):223-34. doi:10.1016/j.immuni.2012.04.015

53. N'Diaye EN, Kajihara KK, Hsieh I, Morisaki H, Debnath J, Brown EJ. PLIC proteins or ubiquilins regulate autophagy-dependent cell survival during nutrient starvation. *EMBO Rep*. Feb 2009;10(2):173-9. doi:10.1038/embor.2008.238

54. Metur SP, Song X, Mehta S, et al. Yeast TIA1 coordinates with Npl3 to promote ATG1 translation during starvation. *Cell Rep*. Jun 24 2025;44(6):115847. doi:10.1016/j.celrep.2025.115847

55. Mao D, Lin G, Tepe B, et al. VAMP associated proteins are required for autophagic and lysosomal degradation by promoting a PtdIns4P-mediated endosomal pathway. *Autophagy*. Jul 2019;15(7):1214-1233. doi:10.1080/15548627.2019.1580103

Figure legends

Figure 1: ALS-RAP targets. (A) Number of PubMed entries related to ALS-RAP genes. Black points represent the number of entries retrieved using the search term "gene name + ALS," while gray points represent entries retrieved using the gene name alone. The x-axis indicates the number of PubMed entries, and the y-axis lists the gene names. **(B)** Heatmap showing normalized RNA expression values from the Human Protein Atlas (HPA) single nuclei brain dataset. Expression is given as nTPM values on a scale from 0-500. Genes denoted with an asterisk (*) indicate "barely detectable" genes with substantial expression in a single cell type.

Figure 2: Summary of antibody performance for ALS-RAP. (A) Overview of the identification of high-quality antibodies for ALS-RAP proteins. **(B)** Clonality of the top- and second-most-cited antibodies. **(C)** Number of citations associated with the top- and second-most-cited antibodies, grouped by antibody type. **(D)** Coverage of ALS-RAP targets across applications, grouped by antibody type. **(E)** Summary of antibodies that were successful in the indicated applications.

Figure 3: Protein expression profiling of 29 ALS-associated proteins. KO-validated antibodies targeting the indicated proteins were selected from antibody characterization reports and used for western blotting. A Ponceau-stained membrane is shown as loading and transfer controls. Lysates were prepared from human iPSC-derived motor, cortical, and dopaminergic neurons, as well as iPSC-derived oligodendrocytes, astrocytes, and microglia. Primary human fetal astrocytes and microglia, along with human monocyte-derived macrophages (MDMs), were also included. [a]=batch A of differentiated neurological cell types or donor A of fetal astrocytes; [a1, a2]= MDMs from two different donors, with a lysate from either donor A1 or A2 used per immunoblot.

Figure 4: RNA sequencing of iPSC-derived microglia.

(A) Analysis of differentially expressed genes (DEGs) upon IFNγ treatment of iPSC-derived microglia was performed using DESeq2, an FDR-adjusted p-value of ≤ 0.05 and log2 fold change of -/+ 0.5 were used to determine significant DEGs. Z-score of DESeq2 normalized counts of all significantly regulated IFNγ DEGs across replicates of vehicle or IFNγ treated iPSC-derived microglia are shown. IFNγ DEGs were broadly grouped (cluster 1-3) based on expression patterns using k-means clustering. **(B)** Over-representation analysis reveals functional annotation of IFNγ DEG clusters. **(C)** Fold change of known IFNγ-responsive genes in IFNγ treated iPSC-derived microglia compared to vehicle treated iPSC-derived microglia. **(D)** Fold change of ALS-RAP genes in IFNγ treated iPSC-derived microglia compared to vehicle treated iPSC-derived microglia. [c]=batch C of differentiated iPSC-derived microglia. * $p \leq 0.05$, ** $p \leq 0.01$, *** $p \leq 0.001$, **** $p \leq 0.0001$

Figure 5: Immune regulation of ALS-RAP proteins. KO-validated antibodies targeting 23 ALS-associated proteins were selected from antibody characterization reports and used for western blotting. iPSC-derived microglia and primary fetal microglia were left non-treated (NT) or were stimulated with IFNγ and LPS, while some iPSC-derived microglia were additionally stimulated with IL-4. Lysates from microglia were analyzed by SDS-PAGE, followed by western blotting with the indicated antibodies. Ponceau-stained membranes are shown as loading and transfer controls. [a]=batch A of differentiated motor neurons; [c]=batch C of differentiated microglia. NT=non-treated or unstimulated.

Figure S1: STRING network analysis. Analysis of known physical interactions between ALS-related proteins.

Figure S2: Repeat of protein expression profiling. As in Figure 3, specific antibodies were used for western blotting, but semi-quantitative fluorescence-based immunoblotting was performed. Lysates were prepared from a different batch of cells than those used in Figure 3. [b]=batch B of differentiated neurological cell types or fetal astrocytes from donor B; [b1,b2]=MDMs from two different donors – a lysate from donor B1 or B2 was used per immunoblot.

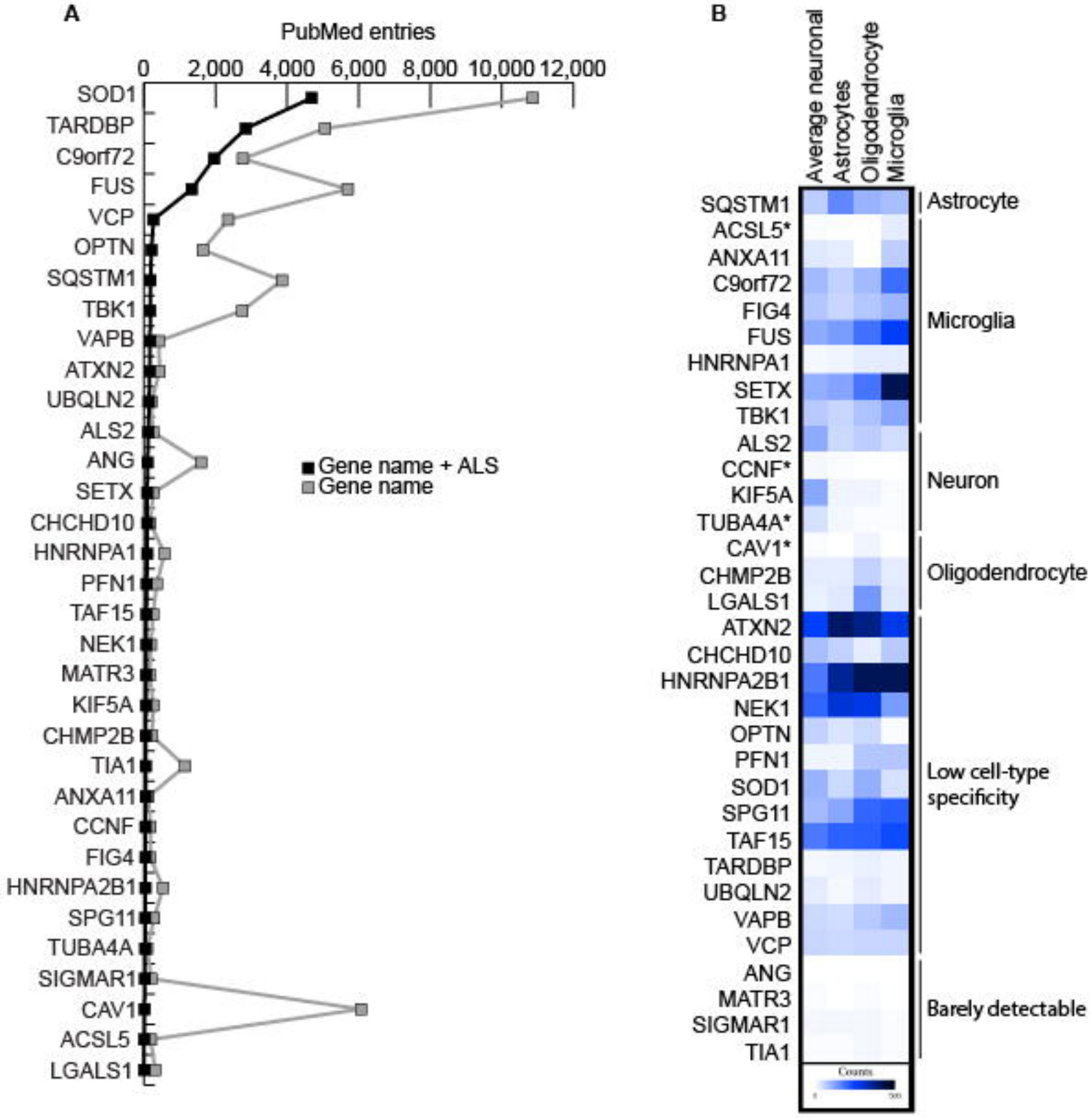

Ayoubi et al., Figure 1

A

gene name	no antibody tested	WB	IP	IF
ACSL5	8	●	●	■
ALS2	3	●	●	⬢
ANG	3	■	⬢	—
ANXA11	15	●	●	⬢
ATXN2	5	●	●	■
C9orf72	16	●	●	●
CAV1	17	●	—	—
CCNF	3	●	—	—
CHCHD10	4	●	●	●
CHMP2B	8	●	●	●
FIG4	5	●	⬢	⬢
FUS	10	●	●	●
HNRNPA1	6	●	⬢	●
HNRNPA2B1	8	●	●	●
KIF5A	4	⬢	—	—
LGALS1	11	●	—	—
MATR3	4	●	●	●
NEK1	9	●	—	—
OPTN	8	●	●	●
PFN1	16	●	●	●
SETX	11	●	—	—
SIGMAR1	5	●	⬢	⬢
SOD1	11	●	●	●
SPG11	3	●	⬢	⬢
SQSTM1	17	●	●	●
TAF15	5	●	●	●
TARDBP	18	●	●	●
TBK1	11	●	●	●
TIA1	12	●	●	●
TUBA4A	6	●	●	●
UBQLN2	10	●	●	●
VAPB	6	●	●	●
VCP	16	●	●	●

● Specific, renewable antibody identified
■ Specific, polyclonal antibody identified
⬢ No specific antibodies identified
— Application not tested

B

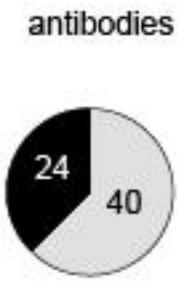

C

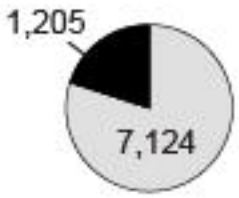

renewable antibodies
polyclonal antibodies

D

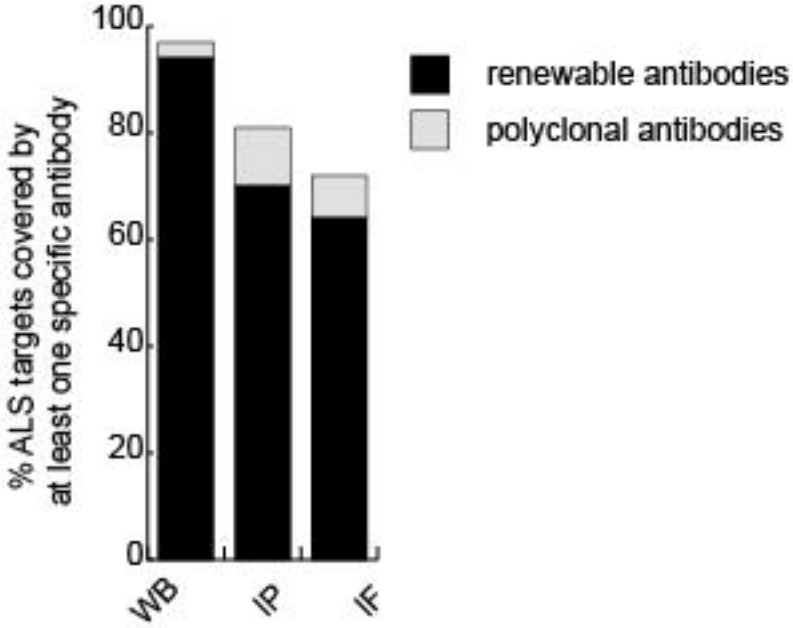

E

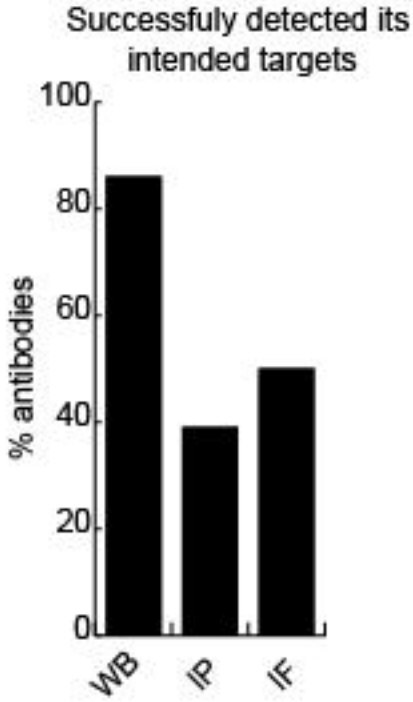

Ayoubi et al., Figure 2

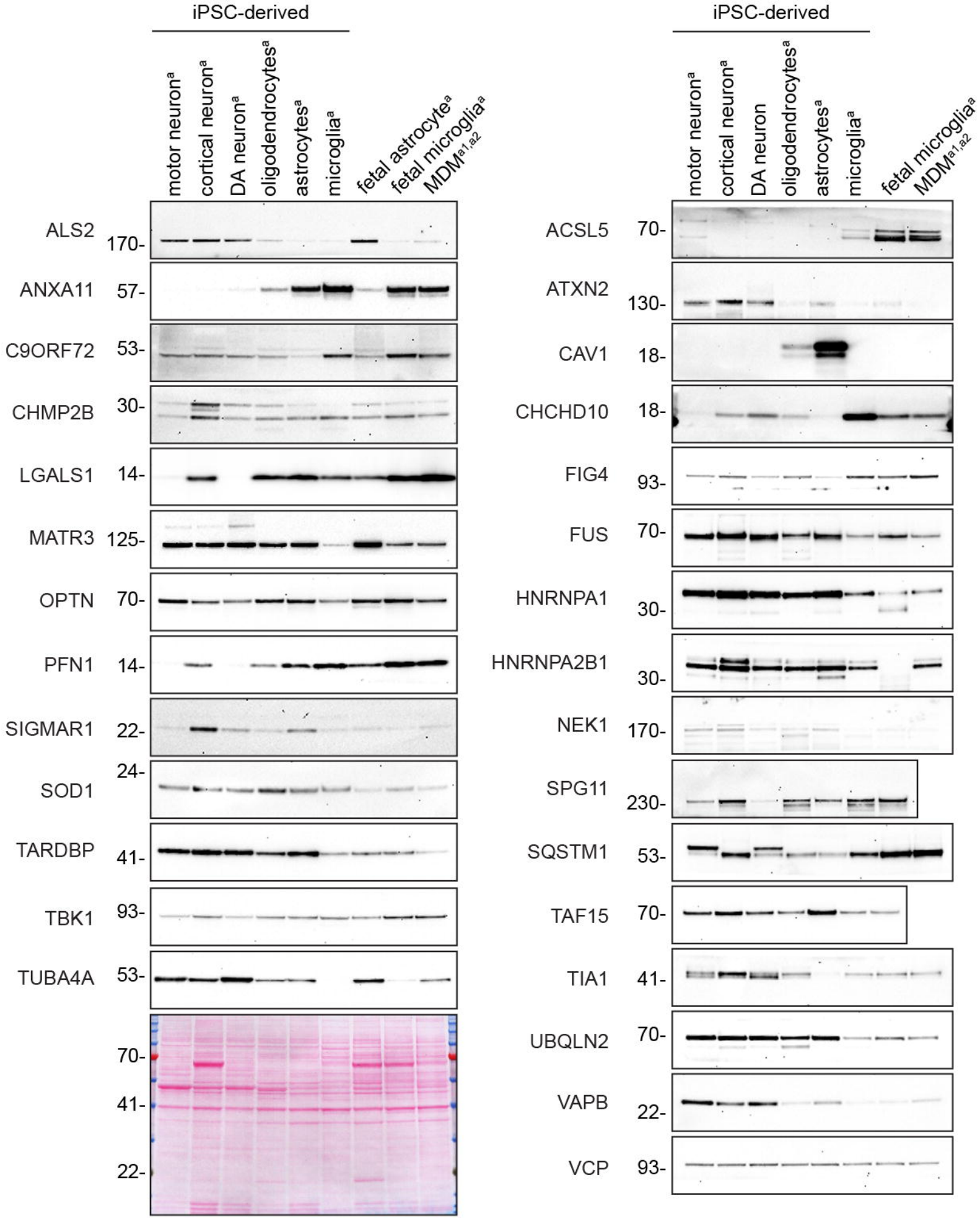

Ayoubi et al., Figure 3

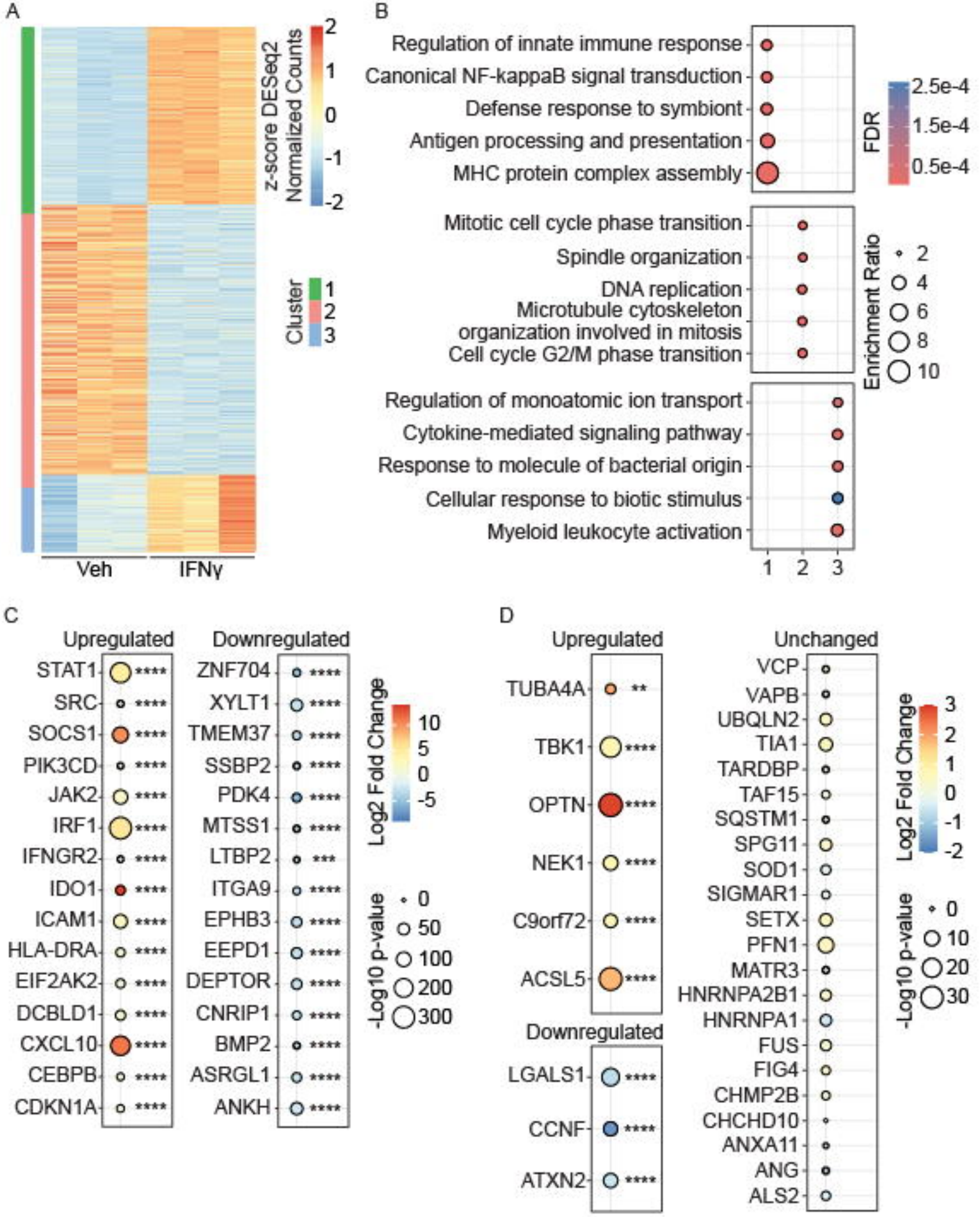

Ayoubi et al., Figure 4

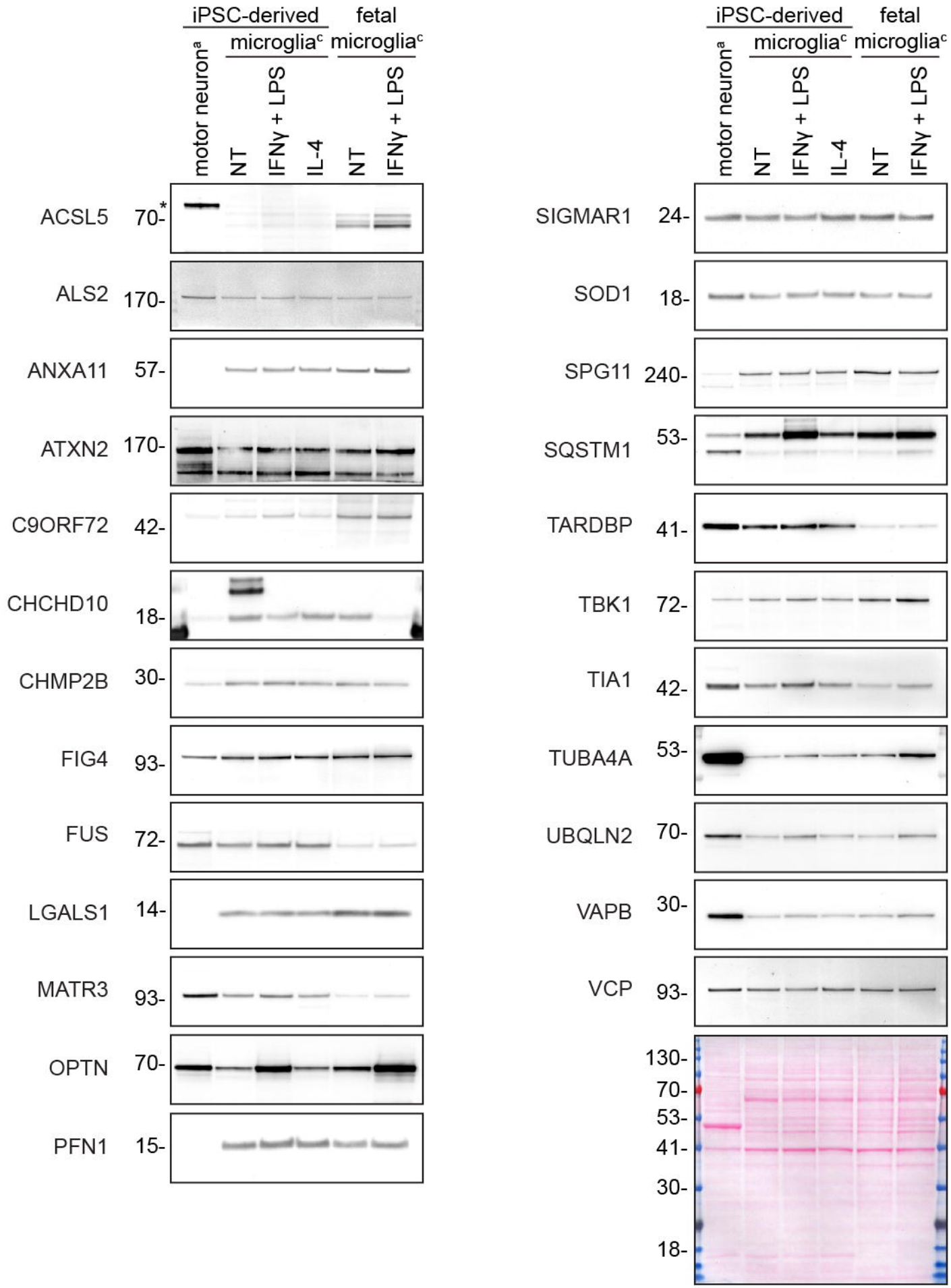

Ayoubi et al., Figure 5

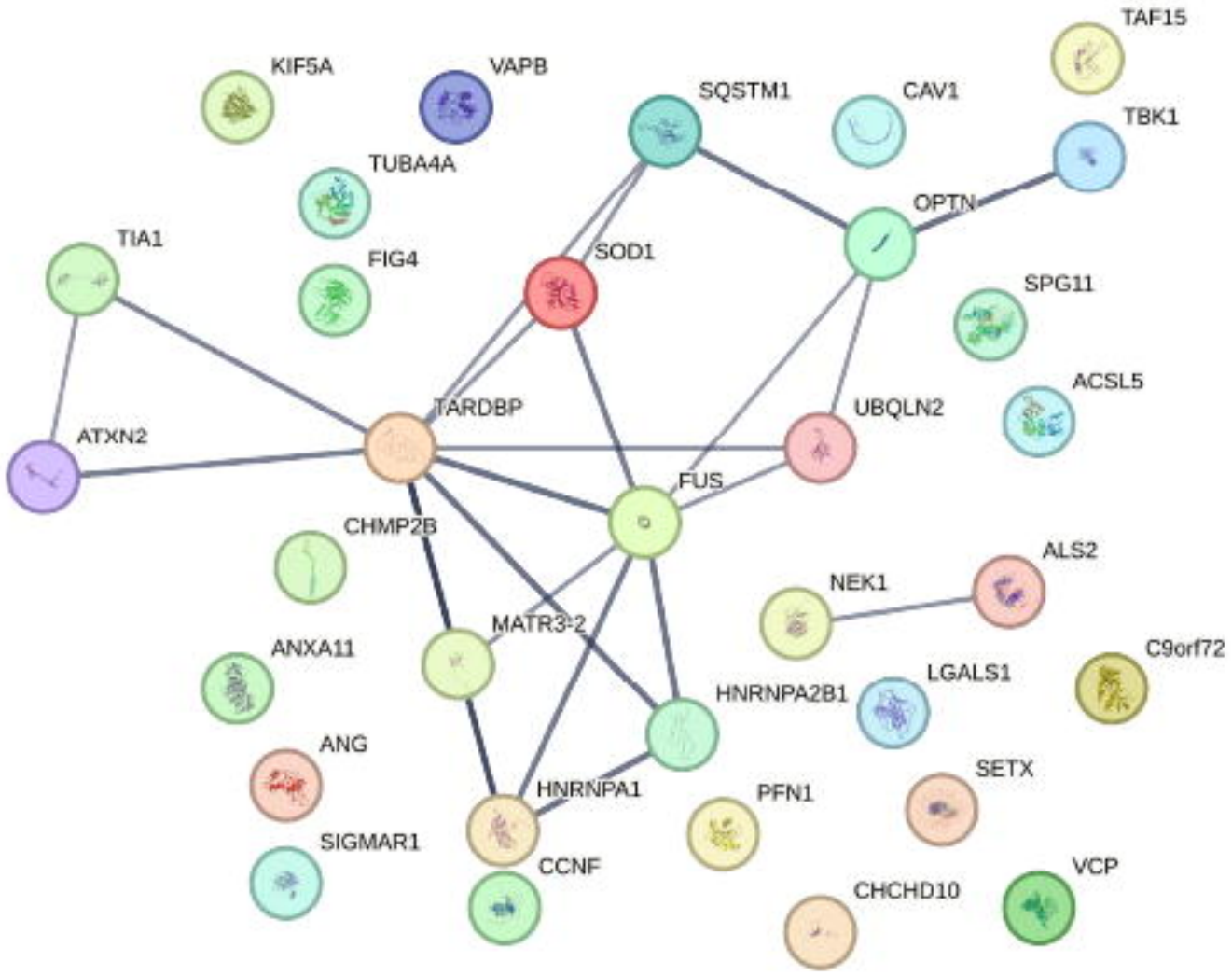

Ayoubi et al., Figure S1

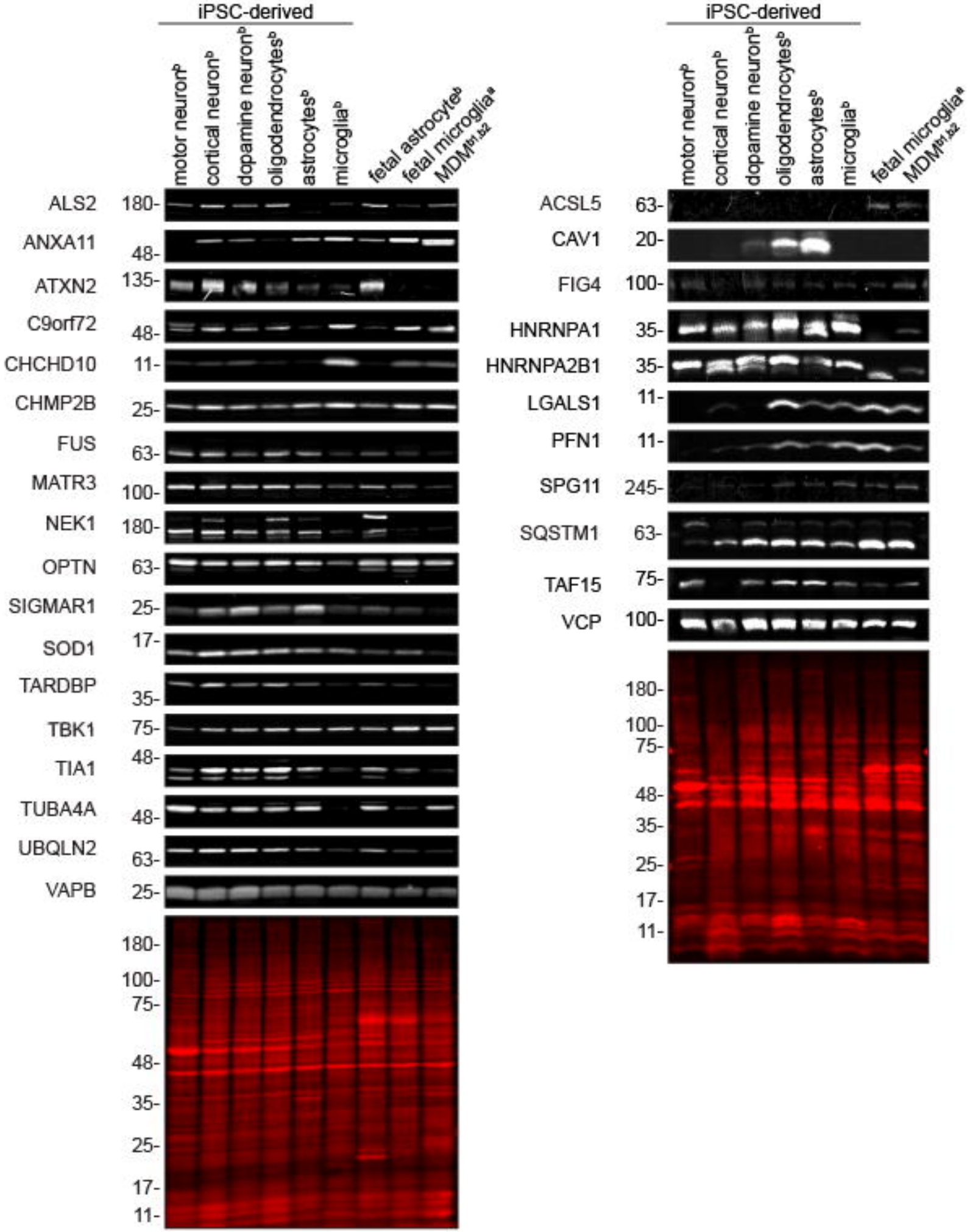

Ayoubi et al., Figure S2